International Scientific Technical and Economic Research
https://doi.org/10.67541/istaer2627
Research Article Volume 4, Issue 3 (July 2026) Open Access

Economic Dispatch Optimization of Microgrid Based on an Improved Particle Swarm Optimization Algorithm

Haoyu You *, **Longtai Hua**, **Tianyi Su**

Department of Electrical and Information Engineering, Shandong University of Science and Technology, Jinan, Shandong, China

***Corresponding author:** Haoyu You. Email: 19953322591@163.com

Abstract

The high proportion of renewable energy access makes the economic dispatch of microgrid face the dual challenges of bilateral source-load uncertainty and high-dimensional nonlinear constraints. The traditional particle swarm optimization algorithm tends to converge prematurely, and its convergence accuracy is insufficient when solving this problem. In this paper, an improved particle swarm optimization (PSO) algorithm is proposed, which integrates a nonlinear adaptive inertia weight, a learning factor dynamic cooperative strategy, and a mutation disturbance mechanism based on population diversity monitoring. The algorithm adjusted the population fitness variance feedback inertia weight, establishes an exploration-development stage criterion based on the evolutionary rate to realize asymmetric cooperation of learning factors, and uses the fitness variance as a premature judgment index to trigger Gaussian mutation disturbance. A typical grid-connected microgrid including photovoltaic, wind power, diesel generator, and energy storage is taken as an example to verify under three scenarios: typical day, high fluctuation day and extreme weather day. The results show that the optimal operating cost of the improved algorithm is 1,983.5 yuan in typical daily scenarios, which is 6.95% lower than that of the standard PSO algorithm. The standard deviation across ten independent runs is 9.8 yuan, which is 56.6% lower than that of the standard algorithm. The source-load bilateral strategy coordination reduces the cost by 8.03%, demonstrating a positive interaction effect. The cost in the extreme weather scenario is 2,851.9 yuan, which is still significantly lower than the comparison algorithm. This study provides an efficient and robust optimization solution for economic dispatch in microgrids under high uncertainty.

Keywords

Microgrid economic dispatch; Improved particle swarm optimization; Inertia weight adaptive; Synergy of learning factors; Premature convergence inhibition

Received: 11 Jul 2026; Revised: 28 Jul 2026; Accepted: 18 Aug 2026; Published: 28 Aug 2026

1. INTRODUCTION

With the increasingly prominent global energy crisis and environmental problems, renewable energy power generation technologies represented by photovoltaic and wind power have achieved rapid development over the past two decades. However, the intermittency and volatility of renewable energy output have brought unprecedented challenges to the safe and stable operation of power systems [1]. As a small power distribution system that organically integrates distributed power supplies, energy storage devices, loads, and control devices, the microgrid can effectively coordinate various types of distributed energy and achieve self-balance and control in local areas, thus becoming an important organizational form of power grid operation under the background of high proportion of renewable energy access [2],[3]. The microgrid can operate in both grid-connected and island modes, showing great application potential in improving power supply reliability, promoting new energy consumption, and reducing power supply costs. With the deepening of power market reform, microgrid operators face the core economic proposition of minimizing operating costs while meeting system security constraints [4],[5]. Therefore, the economic dispatch problem of microgrid has become a research hotspot of common concern in academia and engineering circles.

The economic dispatch of microgrid is essentially a complex optimization problem with multi-period, multi-constraint, and multi-objective characteristics. At the mathematical level, the problem includes the nonlinear fuel cost function of the diesel generator, the time-series coupling constraint of the energy storage system, the power balance constraint, and a large number of inequality boundary constraints, making it a typical nonlinear constrained optimization problem whose feasible region is partitioned into several non-convex sub-regions by high-dimensional constraints. Traditional optimization methods such as linear programming, dynamic programming, and mixed integer programming often suffer from sharp efficiency decline or even infeasibility when the model scale expands or uncertainty factors are introduced [6]. Over the past decade, intelligent optimization methods represented by particle swarm optimization (PSO), genetic algorithms, and differential evolution have been widely used in power system optimization due to their advantages of not relying on gradient information and being easy to parallelize. Among them, the PSO algorithm has a simple structure, fewer parameters, and fast convergence speed, making it especially suitable for solving the economic dispatch problem of microgrids dominated by continuous variables.

Although the PSO algorithm has achieved some results in the economic dispatch of microgrids, a large number of studies have shown that the standard PSO algorithm has inherent defects that cannot be ignored in high-dimensional constrained optimization scenarios [7],[8]. First, the fixed or linear decay settings of the inertia weight cannot match the differentiated requirements for global exploration and local exploitation in different search stages, resulting in the algorithm either prematurely losing the ability to search unvisited areas and falling into local optima, or oscillating around the optimal solution without further improvement. Second, the symmetric and constant values of cognitive and social learning factors make the particles lack a dynamic trade-off mechanism between individual historical experience and group social information. Moreover, when population diversity drops below the critical level, the particle velocity update equation approaches stagnation, while the standard PSO algorithm itself does not have active intervention means to restore population vitality. The above defects are particularly prominent in the economic dispatch problem of microgrids, where the number of decision variables is usually in the tens to hundreds and the feasible region is partitioned into narrow, sparsely distributed sub-regions by multiple constraints.

In view of the above problems, scholars have improved the PSO algorithm from multiple perspectives. In terms of inertia weight adjustment, strategies have evolved from linear decay to dynamic adjustment based on population evolution information and even to adaptive strategies [9]. However, existing dynamic strategies mostly take iterative progress as the single adjustment basis, lacking effective use of information that directly reflects the search state. In terms of learning factors, some studies have proposed schemes in which learning factors change with iterations, but the adjustments of cognitive and social learning factors are often independent of each other, lacking systematic consideration of their synergistic relationship. In terms of population diversity maintenance, previous studies have introduced mutation operators from genetic algorithms, but the trigger timing mostly adopts a fixed period or probability rather than being based on quantitative judgment of whether the population is truly in a premature state. In addition, most improvement studies only modify the standard algorithm from a single strategy, lacking the co-design of inertia weight, learning factors, and diversity maintenance mechanisms [10].

Aiming at the above research gaps, this paper proposes an improved particle swarm optimization algorithm (IPSO-IE) that integrates a nonlinear adaptive inertia weight, a dynamic cooperative strategy of learning factors, and a mutation disturbance mechanism based on population diversity monitoring, and applies it to the multi-source coordinated economic dispatch problem of microgrids. Specifically, this paper constructs a multi-source economic dispatch model including photovoltaic, wind power, diesel generator and energy storage system. Accurate photovoltaic power generation prediction is essential for the economic dispatch of microgrids, and deep learning-based prediction models have shown promising performance in this domain. The scenario method combining Latin hypercube sampling and K-means clustering is used to transform stochastic optimization into deterministic optimization [11],[12]. Then, based on the convergence analysis of standard PSO, the nonlinear adaptive inertia weight function is designed to respond to both iterative process and population fitness variance. An asymmetric cooperative adjustment scheme of cognitive and social learning factors is constructed, and an "exploration-development" stage conversion criterion based on evolutionary rate is introduced. The population fitness variance is defined as the quantitative index for premature convergence determination, and Gaussian mutation disturbance with iteration-decaying probability is introduced. Finally, through multi-group comparison experiments, ablation experiments and parameter sensitivity analysis under typical daily, high fluctuation and extreme weather scenarios, the advantages of the improved algorithm in convergence accuracy, solution stability and adaptability to uncertainty are systematically verified. The research results can provide an efficient and robust optimization solution tool for the day-ahead economic dispatch of microgrid and have certain theoretical significance and engineering reference value for promoting the economic and efficient operation of microgrid with high proportion of renewable energy.

2. MULTI-SOURCE COORDINATED ECONOMIC DISPATCH MODEL OF MICROGRID

As the key interface between distributed energy and distribution network, microgrid contains various types of distributed power generation units and energy storage devices, and each unit has significant differences in physical characteristics, control mode and operating cost. In order to optimize the overall operating economy of the system, it is necessary to establish a mathematical description system that can accurately reflect the output characteristics of each unit and the coupling relationship between the units. This section takes a typical grid-connected AC microgrid as the research object, systematically constructs a multi-source coordinated economic dispatch model including photovoltaic power generation, wind power generation, diesel generator and energy storage battery, and gives a complete mathematical framework of multi-scenario deterministic transformation from the perspective of bilateral uncertainty of source and charge.

2.1 Modeling of microgrid system topology and component units

2.1.1 System topology

The microgrid system studied in this paper adopts AC bus structure, photovoltaic array and wind turbine are connected to AC bus through DC-DC converter and AC-DC converter, energy storage system realizes energy exchange with AC bus through bidirectional DC-AC converter, diesel generator is directly connected to the grid through synchronous generator as controllable power supply, load takes power from AC bus through feeder [13],[14]. The system is connected to the external distribution network through the common coupling point to form a grid-connected microgrid with bidirectional energy flow.

2.1.2 Photovoltaic power generation output model

The output power of photovoltaic array mainly depends on the solar radiation intensity and ambient temperature. Under standard working conditions, the output current and voltage of photovoltaic cells show a nonlinear relationship. Based on the simplified requirements in practical engineering applications, this paper adopts the photovoltaic output prediction model, and expresses the output power of photovoltaic array at a certain time as [15],[16]:

$$P_{PV}(t) = P_{PV,STC} \cdot \frac{G(t)}{G_{STC}} \cdot [1 + \alpha_T(T_c(t) - T_{STC})] \tag{1}$$

Where, $P_{PV,STC}$ is the rated output power of photovoltaic array under standard test conditions (irradiance $G_{STC} = 1000$ W/m^2, battery temperature $T_{STC} = 25$°C), $G(t)$ is the actual irradiance at time t, α_T is the power temperature coefficient (usually taken from -0.0035 to -0.0045 /°C), and $T_c(t)$ is the actual working temperature of the PV cell at time t. Due to the inherent deviation of the irradiancy prediction provided by numerical weather prediction, the actual power output is not a definite value. Therefore, the concept of prediction interval is introduced to describe the uncertainty. $P_{PV}(t)$ can be regarded as a random variable that follows a certain probability distribution around the predicted value $\hat{P}_{PV}(t)$, and the width of the confidence interval is determined by the statistical characteristics of the prediction error.

2.1.3 Wind power output model

There is a clear functional relationship between the output power of the wind turbine and the wind speed at the hub height. When the wind speed is between the cut wind speed and the rated wind speed, the output power is approximately a cubic function of the wind speed. When the wind speed reaches the rated wind speed to the cut out wind speed interval, the output power is maintained at the rated value; When the wind speed exceeds the cutting speed, the fan shall implement the cutting machine protection. The segmentation feature can be expressed as:

$$P_{WT}(t) = \begin{cases} 0, & v(t) < v_{ci} \text{ or } v(t) \geq v_{co} \\ P_{WT,rated} \cdot \dfrac{v^3(t) - v_{ci}^3}{v_{rated}^3 - v_{ci}^3}, & v_{ci} \leq v(t) < v_{rated} \\ P_{WT,rated}, & v_{rated} \leq v(t) < v_{co} \end{cases} \tag{2}$$

Where $v(t)$ is the actual wind speed at the hub height at time t; v_{ci}, v_{rated} and v_{co} are the cut in wind speed, rated wind speed and cut out wind speed respectively; $P_{WT,rated}$ is the rated power of the fan. Because there are also significant uncertainties in wind speed prediction, especially when the local micrometeorological conditions change rapidly, the prediction error is more prominent, so $P_{WT}(t)$ is also treated as a random variable with prediction interval.

2.1.4 Fuel cost model of diesel generator

As the only completely controllable power source in the microgrid, the output of diesel generator can be continuously adjusted within a certain range, but there is a nonlinear growth relationship between generation cost and output. The relationship between fuel consumption $F_{\mathrm{DE}}(t)$ and active power output $P_{\mathrm{DE}}(t)$ is usually fitted by quadratic polynomial, and the corresponding fuel cost function is written as follows [17]:

$$C_{\mathrm{DE}}(t) = a \cdot P_{\mathrm{DE}}^{2}(t) + b \cdot P_{\mathrm{DE}}(t) + c \tag{3}$$

Where a, b and c are the fuel cost coefficients of the diesel generator, and the unit is yuan/kW$^2 \cdot$ h, yuan/kW $\cdot$ h and yuan/h, corresponding to the quadratic term coefficient, the primary term coefficient and the fixed cost coefficient respectively. It should be pointed out that c reflects the basic fuel consumption of the diesel generator in no-load operation. Even if the output is zero, this part of the cost still exists. This feature makes the unit power generation cost of the diesel generator in low-load condition significantly higher than the rated condition, so it is not suitable for frequent start and stop or long-term operation in light load state.

2.1.5 Operation model of energy storage system

Energy storage system plays a dual role of peak cutting and valley filling and power fluctuation suppression in microgrid. In this paper, lithium-ion battery is used as energy storage carrier, and its operation characteristics are described by two core state quantities: state of charge and charge and discharge power. The state of charge $S_{\mathrm{OC}}(t)$ at time t is defined as the ratio of current remaining capacity to rated capacity:

$$S_{\mathrm{OC}}(t) = \frac{E(t)}{E_{\mathrm{rated}}} \tag{4}$$

Where $E(t)$ is the residual power (unit: kWh) of the energy storage system at time t, and E_{rated} is the rated capacity is. There is an efficiency loss in energy conversion of energy storage systems during charging and discharging, and its discrete time recurrence relation is as follows [18]:

$$E(t+1) = E(t) + \eta_{\mathrm{ch}} \cdot P_{\mathrm{ch}}(t) \cdot \Delta t - \frac{P_{\mathrm{dis}}(t)}{\eta_{\mathrm{dis}}} \cdot \Delta t \tag{5}$$

Where, $P_{\mathrm{ch}}(t)$ and $P_{\mathrm{dis}}(t)$ are the charging power and discharging power (unit: kW) at time t, η_{ch} and η_{dis} represent the charging efficiency and discharging efficiency, and Δt is the scheduling step length (1 hour). In order to avoid over-charge or over-discharge of the energy storage system, the state of charge must always be maintained within the safe operation interval, that is, $S_{\mathrm{OC,min}} \le S_{\mathrm{OC}}(t) \le S_{\mathrm{OC,max}}$, and the charging and discharging power is limited by the rated capacity of the energy storage converter. Meet $0 \le P_{\mathrm{ch}}(t) \le P_{\mathrm{ch,max}}$ and $0 \le P_{\mathrm{dis}}(t) \le P_{\mathrm{dis,max}}$. In order to quantify the life loss cost of energy storage system in charge and discharge cycle, this paper adopts the equivalent depreciation cost model to convert the equivalent depreciation cost of a single charge and discharge cycle to the unit discharge quantity, which is specifically expressed as:

$$C_{\mathrm{BESS}} = \sum_{t=1}^{T} \left(\lambda_{\mathrm{deg}} \cdot \frac{P_{\mathrm{dis}}(t) \cdot \Delta t}{D_{\mathrm{OD}}} \right) \tag{6}$$

Where λ_{deg} is the depreciation factor of energy storage unit throughput (unit: yuan /kWh), and its value is determined based on the ratio of the total throughput of battery life cycle to the initial investment cost; D_{OD} is the correction coefficient of discharge depth, which is used to reflect the difference of cycle life under different discharge depth.

2.2 Multi-objective optimal scheduling model

2.2.1 Economic objective function

The primary objective of economic dispatch in a microgrid is to minimize the total operating cost of the system during the dispatch period. The total operating cost covers the fuel consumption cost of the diesel generator, the cyclic depreciation cost of the energy storage system, and the power exchange cost between the microgrid and the external distribution network. The link line exchange cost consists of electricity purchase cost and electricity sales income. When the internal power generation of the microgrid is insufficient to meet the load demand, electricity purchase cost will be generated from the main grid. When there is surplus in internal power generation, electricity is sold to the main grid, and the revenue from electricity sales is obtained (reflected in the objective function as a negative cost term). The complete form of the economic objective function is:

$$F_1 = \sum_{t=1}^{T} \left[C_{\mathrm{DE}}(t) + C_{\mathrm{BESS}}(t) + C_{\mathrm{grid}}(t) \right] \tag{7}$$

Where T is the total number of periods in the scheduling cycle (24 in this paper), and $C_{\mathrm{grid}}(t)$ represents the power exchange cost between the microgrid and the main grid at time t, which is defined as:

$$C_{\mathrm{grid}}(t) = \begin{cases} p_{\mathrm{buy}}(t) \cdot P_{\mathrm{buy}}(t) \cdot \Delta t, & P_{\mathrm{grid}}(t) \geq 0 \\ -p_{\mathrm{sell}}(t) \cdot P_{\mathrm{sell}}(t) \cdot \Delta t, & P_{\mathrm{grid}}(t) < 0 \end{cases} \tag{8}$$

Where $P_{\mathrm{grid}}(t)$ is the exchange power of the tie line (positive value is electricity purchased, negative value is electricity sold), $P_{\mathrm{buy}}(t)$ and $P_{\mathrm{sell}}(t)$ are the absolute values of electricity purchased and sold respectively, $p_{\mathrm{buy}}(t)$ and $p_{\mathrm{sell}}(t)$ are the purchase price and sale price of electricity at time t, respectively.

2.2.2 Environmental protection objective function

Under the background of "dual carbon", in addition to the consideration of economy, the constraint consideration of pollutant emission should also be included in the dispatching decision of microgrid. The emissions of carbon dioxide, sulfur oxides and nitrogen oxides from diesel generators in the process of burning diesel to generate electricity have a significant impact on the environment. In this paper, the emission conversion cost method is adopted to multiply the emission of various pollutants by the corresponding environmental value cost coefficient and convert them into quantifiable environmental protection targets:

$$F_2 = \sum_{t=1}^{T} \left[\beta_{\mathrm{CO_2}} \cdot E_{\mathrm{CO_2}}(t) + \beta_{\mathrm{SO_2}} \cdot E_{\mathrm{SO_2}}(t) + \beta_{\mathrm{NO}_x} \cdot E_{\mathrm{NO}_x}(t) \right] \tag{9}$$

Where $E_{\mathrm{CO_2}}(t)$, $E_{\mathrm{SO_2}}(t)$, and $E_{\mathrm{NO}_x}(t)$ are the mass of carbon dioxide, sulfur dioxide and nitrogen oxide emitted by the diesel generator at time t, respectively. $\beta_{\mathrm{CO_2}}$, $\beta_{\mathrm{SO_2}}$, β_{NO_x} as the corresponding unit mass of pollutants environmental value cost. The relationship between various types of emissions and the output of diesel generators is determined by the emission coefficient method, that is, the emission factor corresponding to the unit of power generation multiplied by the actual power generation.

2.2.3 Multi-objective processing strategy

The economic objective F_1 and the environmental objective F_2 form a set of conflicting multi-objective optimization problems in mathematics. In this paper, the linear weighted combination method is used to transform the dual objective into the single objective function:

$$F = \omega_1 \cdot \tilde{F}_1 + \omega_2 \cdot \tilde{F}_2 \tag{10}$$

Type of $\tilde{F}_1$ and $\tilde{F}_2$ respectively two objective functions after normalization treatment of dimensionless value of ω_1 and ω_2 as weight coefficient, satisfy the $\omega_1 + \omega_2 = 1$ and $\omega_1, \omega_2 \in [0, 1]$. The ideal point method is used for normalization, and the optimal value obtained when each objective is optimized separately is used as the benchmark for standard unitary. The selection of weight coefficients reflects the relative preference of decision makers for economy and environmental protection, and this paper will set multiple groups of weight combinations for analysis in subsequent experiments.

2.2.4 Constraint condition system

The economic dispatch of microgrid needs to be optimized in the feasible region formed by the following constraints. The first is the power balance constraint, which requires that the sum of the output of each power generation unit and the charging and discharging power of energy storage is equal to the net value of the load demand and the exchange power of the tie line at the moment:

$$P_{\mathrm{PV}}(t) + P_{\mathrm{WT}}(t) + P_{\mathrm{DE}}(t) + P_{\mathrm{dis}}(t) - P_{\mathrm{ch}}(t) + P_{\mathrm{grid}}(t) = P_{\mathrm{load}}(t) \tag{11}$$

Where $P_{\mathrm{load}}(t)$ is the total load power of the microgrid at time t. Secondly, the upper and lower limits of the output of each unit are constrained. The output of diesel generator should be located between its minimum stable output and rated output:

$$P_{\mathrm{DE,min}} \leq P_{\mathrm{DE}}(t) \leq P_{\mathrm{DE,max}} \tag{12}$$

The energy storage system must satisfy both the state of charge boundary constraint and the charge and discharge power boundary constraint, which is given in Section 2.1.5. The tie-line interactive power is limited by the grid-connected transformer capacity and the maximum switching capacity specified in the grid access agreement:

$$-P_{\mathrm{grid,max}} \leq P_{\mathrm{grid}}(t) \leq P_{\mathrm{grid,max}} \tag{13}$$

In addition, the climbing rate constraint of diesel generators is also taken into account, limiting the variation range of output in adjacent periods to no more than the maximum climbing rate:

$$|P_{\mathrm{DE}}(t) - P_{\mathrm{DE}}(t-1)| \leq R_{\mathrm{DE,max}} \cdot \Delta t \tag{14}$$

Where $R_{\mathrm{DE,max}}$ is the maximum climbing rate of the diesel generator (unit: kW/h).

2.3 Bilateral uncertainty treatment of source charge

2.3.1 Scene generation based on Latin Hypercube sampling

The uncertainty of scenery output comes from the inherent randomness of meteorological forecast errors. Using the deterministic forecast value as the scheduling basis will lead to the deviation between the planned output and the actual available output, which will affect the strict satisfaction of the power balance constraint. In order to effectively depict this uncertainty, this paper uses Latin hypercube sampling method to generate a large number of equal probability scenarios in the distribution space of scenery prediction errors.

Set up photovoltaic output prediction error of $\varepsilon_{\mathrm{PV}}$ obey the mean, standard deviation is zero for σ_{PV} of the normal distribution, namely the $\varepsilon_{\mathrm{PV}} \sim \mathcal{N}(0, \sigma_{\mathrm{PV}}^2)$; The wind speed prediction error ε_{v} follows $\mathcal{N}(0, \sigma_{\mathrm{v}}^2)$, which indirectly affects the distribution of P_{WT} through the fan power curve mapping. The core idea of Latin hypercube sampling is to divide the cumulative distribution function of each random variable into N_{s} non-overlapping intervals with equal probability, select a sample point from each interval with equal probability, and then randomly combine the samples of each variable. Compared with simple random sampling, Latin hypercube sampling achieves uniform coverage of the entire distribution space with fewer sampling times. For M uncertain variables, each column of the sampling matrix $X \in \mathbb{R}^{N_{\mathrm{s}} \times M}$ represents N_{s} sampling values of a certain variable, and the row vector constitutes a complete scene. After this step, N_{s} initial scenarios are obtained, and each scenario contains P_{PV} and P_{WT} trajectories for each period of the complete scheduling cycle.

2.3.2 Scene reduction based on K-means clustering

The number of initially generated scenarios is large, and directly substituting the scheduling model for scene-by-scene optimization will lead to exponential growth of calculation, which cannot meet the real-time requirements of the project. Therefore, it is necessary to effectively compress the scene without significant loss of distribution information. In this paper, the k-means clustering algorithm is used to cluster and merge N_{s} initial scenes and finally condensed into K typical scenes (usually $K = 5$ to 10). K-means clustering uses the Euclidean distance between scenes as the similarity measure, and the objective function is to minimize the sum of squares of the distance between each scene and the center of the cluster [19],[20]:

$$J = \sum_{k=1}^{K} \sum_{x \in C_k} \|x - \mu_k\|_2^2 \tag{15}$$

Where C_k is the scene set of the k-th cluster, and μ_k is the center vector of the cluster. After the clustering is completed, each typical scene μ_k is assigned a probability weight π_k, whose value is the proportion of the number of original scenes contained in the cluster to N_{s}. In this way, the continuous uncertain distribution is transformed into a finite discrete scene set $\{(\mu_k, \pi_k)\}_{k=1}^{K}$, which provides an input for the subsequent multi-scene deterministic optimization.

2.3.3 Load-side demand response model

Different from the traditional power system, which regards load as rigid demand, part of load in microgrid can participate in demand response through price signal or incentive measures, so as to improve the economy of system operation and the adaptability to uncertainty. In this paper, the demand response model based on TOU electricity price is adopted, and the price elasticity matrix is introduced to describe the response of users' electricity consumption behavior to electricity price. The price elasticity coefficient of the demand side is defined as follows:

$$\varepsilon_{ij} = \frac{\Delta P_{\text{load}}(i)/P_{\text{load}}^{0}(i)}{\Delta p(j)/p^{0}(j)} \tag{16}$$

Where ε_{ij} represents the influence degree of electricity price change in period j on load demand in period i, $P_{\text{load}}^{0}(i)$ is the baseline load in period i, $p^{0}(j)$ is the baseline electricity price in period j, $\Delta P_{\text{load}}(i)$ and $\Delta p(j)$ are the load adjustment and the electricity price adjustment, respectively. The elasticity coefficient is divided into self-elasticity coefficient ($i = j$, usually negative) and cross-elasticity coefficient ($i \neq j$, usually positive, reflecting the shift of load from high-priced to low-priced periods). Based on the elasticity matrix, the response afterload in each period can be expressed as:

$$P_{\text{load}}(i) = P_{\text{load}}^{0}(i) \cdot \left[1 + \sum_{j=1}^{T} \varepsilon_{ij} \cdot \frac{\Delta p(j)}{p^{0}(j)}\right] \tag{17}$$

The above formula integrates the dynamic time division strategy into the construction of the elasticity matrix, that is, the scheduling period is divided into three types of time periods according to the load characteristics: peak, flat and valley, and the elastic coefficient in the same type of time period is taken as the same value, so as to reduce the dimension of the model and retain the load transfer characteristics between times.

2.3.4 Multi-scenario deterministic transformation strategy

By integrating the power side scenario set and load side response model, the original stochastic optimization problem with uncertainty is transformed into a multi-scenario deterministic optimization problem. The objective function value corresponding to each typical scene k is $F^{(k)}$, and the final optimization objective takes the expected value of the objective function of each scene:

$$\min \mathbb{E}[F] = \sum_{k=1}^{K} \pi_k \cdot F^{(k)} \tag{18}$$

The power balance constraint must be satisfied in each scenario, that is, for each k and each time period t:

$$P_{\text{PV}}^{(k)}(t) + P_{\text{WT}}^{(k)}(t) + P_{\text{DE}}^{(k)}(t) + P_{\text{dis}}^{(k)}(t) - P_{\text{ch}}^{(k)}(t) + P_{\text{grid}}^{(k)}(t) = P_{\text{load}}^{(k)}(t) \tag{19}$$

It is worth noting that the output of diesel generator and the charging and discharging strategy of energy storage are used as decision variables. Although they can be valued differently in different scenarios, which is equivalent to the adaptive scheduling strategy under uncertainty, the scheduling decision in actual operation needs to be made according to the forecast information in the day-ahead stage. Therefore, this paper adopts the two-stage stochastic programming framework. The day-ahead scheduling plan is determined in the first stage, and the correction and adjustment are made in the second stage according to the actual scenario. The deviation between the two is included in the objective function through the penalty term. Through the above processing, the stochastic optimization problem that cannot be directly solved is transformed into a deterministic large-scale optimization problem that can be efficiently solved by the improved particle swarm optimization algorithm. The total number of decision variables in the model is $K \times T$ (P_{DE}, P_{ch}, P_{dis}, P_{grid} in each scene and each time period). The total number of constraints is $K \times T$ power balance equality constraints and some inequality constraints, which constitutes a complete mathematical programming model of multi-source coordinated economic dispatch of microgrid. Table 1 lists the main technical parameters of each distributed unit in the microgrid studied in this paper, where the conversion efficiency of photovoltaic array refers to the photoelectric conversion efficiency under standard working conditions, the efficiency of wind turbine refers to the comprehensive efficiency of gearbox and generator, the efficiency of diesel generator refers to the thermal efficiency under rated working conditions, and the charging and discharging efficiency of energy storage system is given respectively.

Table 1. Main technical parameters of each distributed unit of the microgrid

Type of cell	Rated power /kW	Minimum stable output /kW	Climbing rate/(kW/h)	Operating efficiency /%
Photovoltaic array	150	—	—	16.5
Wind power generating unit	100	—	—	92.0
Diesel fuel generator	200	40	80	38.5
Energy storage system	100	—	50 (Charge and discharge)	92.0 (charge) /94.0 (discharge)

The constraint of the climbing rate of the diesel generator is 80 kW/h, that is, the adjustment range of the output in the adjacent dispatch period does not exceed this value. The rated capacity of the energy storage system is set to 400 kWh, and the lower limit and upper limit of the state of charge operating interval are set to 0.15 and 0.95, respectively, to ensure battery safety and extend service life. Table 2 shows the emission coefficients of various pollutants corresponding to the unit power generation of diesel generators and their unit price of environmental value costs.

Table 2. Diesel generator emission coefficient and environmental cost unit price

Type of emissions	Emission factor /(g/kWh)	Environmental cost unit price / (Yuan /g)
CO_2	650	0.00025
SO_2	2.8	0.00650
NOx	4.2	0.00800

The emission factor is taken from the average emission level of a typical medium-speed diesel engine in the common load range (50% to 80% rated output). The unit price of environmental cost is converted by referring to the domestic carbon trading market and the trading price of emission rights, and the data in the table are used for quantitative calculation of the corresponding terms of E and β in the environmental protection objective function.

3. IMPROVE THE DESIGN OF PARTICLE SWARM OPTIMIZATION ALGORITHM

The standard particle swarm optimization algorithm has been widely used in the field of power system optimization scheduling because of its simple structure, few parameters and easy to implement. However, the economic dispatch problem of microgrid has the characteristics of high dimension of decision variables (involving multi-period, multi-unit and multi-scene coupling), complex constraints and non-convex objective function. Standard PSO algorithm exposes the inherent defects of insufficient convergence accuracy and premature convergence when solving this kind of problem. In this section, a systematic algorithm improvement scheme is proposed from the three levels of adaptive regulation of inertia weight, co-evolution of learning factors and population diversity maintenance, and the theoretical validity of the improved strategy is verified through convergence analysis and computational complexity evaluation.

3.1 Standard particle swarm optimization algorithm and its convergence analysis

The standard particle swarm optimization algorithm (PSO) is derived from the simulation of bird group foraging behavior. It regards each potential solution of the problem to be optimized as a particle in the search space, and the particle iteratively updates its flight speed and spatial position by tracking the individual historical optimal position and the global optimal position of the group. Let the dimension of the search space be D, the population size be N, and the position vector of the i-th particle in the k-th iteration be expressed as $x_i^k = \left(x_{i,1}^k, x_{i,2}^k, \dots, x_{i,D}^k\right)$, the velocity vector is $v_i^k = \left(v_{i,1}^k, v_{i,2}^k, \dots, v_{i,D}^k\right)$. In the $k+1$ iteration, the velocity and position of the particle are updated according to the following rules:

$$v_i^{k+1} = \omega v_i^k + c_1 r_1\left(p_i^k - x_i^k\right) + c_2 r_2\left(g^k - x_i^k\right) \tag{20}$$

$$x_i^{k+1} = x_i^k + v_i^{k+1} \tag{21}$$

Where ω is the inertia weight, which is used to control the influence degree of the previous speed of the particle on the current flight direction; c_1 and c_2 are cognitive learning factors and social learning factors respectively, which represent the degree of trust of particles in their own historical experience and the adoption intensity of group social information respectively. r_1 and r_2 are independent random numbers, which obey uniform distribution in the interval $[0, 1]$. p_i^k is the individual historical optimal position of the i-th particle up to the k-th iteration, and g^k is the global optimal position of the whole population up to the k-th iteration. The right-hand side of the velocity update equation is composed of three items. The first item is the inertia item, which gives the particle the tendency of continuous flight along the original direction. The second term is the cognitive term, which guides the particle to return to its historical optimal region. The third term is the social term, which drives the particles closer to the global optimum region found by the group. The synergy between the three terms determines the search trajectory of the particle in the solution space.

Inertia weight ω usually adopts a linear decreasing strategy in standard PSO, that is, it linearly decays from the initial value $\omega_{\max}$ to the final value $\omega_{\min}$ [21],[22]. Its mathematical form is:

$$\omega(k) = \omega_{\max} - (\omega_{\max} - \omega_{\min}) \cdot \frac{k}{K_{\max}} \tag{22}$$

Where $K_{\max}$ is the maximum number of iterations. This strategy maintains a large value of ω in the early stage of the algorithm to ensure the global exploration ability and gradually decreases ω with the advance of iteration to enhance the local fine search. The learning factors c_1 and c_2 are usually constant $c_1 = c_2 = 2.0$ in the standard version, which is derived from the theoretical analysis of algorithm stability. In terms of population topology, all particles in the global version of PSO directly communicate with the global optimal particle, so the information propagation speed is fast, but the population diversity is lost rapidly. In the local version of PSO, particles only communicate with particles in the topological neighborhood, so information propagation is slow, but diversity is better maintained.

From the perspective of convergence, the convergence behavior of PSO algorithm can be described by deterministic difference equation. When the random term is ignored, the trajectory of a single particle satisfies the second-order linear difference equation, and the modulus length of its characteristic root determines whether the particle converges to the equilibrium point. When ω, c_1 and c_2 satisfy $c_1 + c_2 > 0$ and $\omega < 1$, the particle trajectories show oscillatory convergence without random disturbances. However, the existence of random terms makes the particles unable to strictly converge to a single equilibrium point but form a probability distribution around the equilibrium point. More importantly, when c_1 and c_2 are symmetric constants, the tendency of particles between cognitive experience and social information does not change with the search process. As a result, once the particles approach a local optimal region in the later stage of the algorithm, the dominant role of social terms will rapidly compress the population diversity, making the particle swarm lose the ability to jump out of the local trap. For high-dimensional constrained optimization problems such as economic dispatch of microgrid, the dimension of decision variable $D = K \times T \times N_{\text{var}}$ is usually up to hundreds or even thousands, and the feasible region is cut into several disconnected sub-regions by a large number of equality constraints and inequality constraints. In such a complex search space, standard PSO frequently produces infeasible solutions due to the lack of directional guidance to the constraint boundary on the one hand, and the single linear decay of inertia weight cannot adapt to the differentiated needs of different search stages on the other hand, resulting in the convergence accuracy is difficult to meet the expected value of engineering applications.

3.2 Algorithm improvement strategy

Aiming at the defects of premature convergence and insufficient convergence accuracy exposed by standard PSO in solving the economic dispatch problem of microgrid, this section proposes a collaborative improvement scheme from three levels, and each improvement strategy complements each other rather than simply superposes, forming a set of algorithm enhancement framework with internal logical consistency.

Improvement points 1: nonlinear adaptive inertia weight adjustment mechanism

The linear decreasing inertia weight strategy forcibly binds the evolution of ω to iterative algebra and ignores the dynamic demand of inertia strength for the actual search state of the population. When the algorithm searched for the better region in the early and middle period, the linearly decreasing inertia weight still maintains a high global search tendency, resulting in unnecessary waste of computing resources. On the contrary, if the algorithm is still far from the global optimum in the middle and late period, too small inertia weight will seriously limit the exploration range of particles, so that they cannot cover the area that has not been visited. This paper proposes a nonlinear adaptive inertia weight adjustment function based on evolution algebra and population fitness concentration degree. The core idea is to make the value of ω respond to both the iterative process and the real-time state of population fitness distribution:

$$\omega(k) = \omega_{\min} + (\omega_{\max} - \omega_{\min}) \cdot \exp\left[-\alpha \cdot \left(\frac{k}{K_{\max}}\right)^{\beta} \cdot \left(1 + \gamma \cdot \sigma_f^2(k)\right)\right] \tag{23}$$

Where α, β and γ are the adjustment coefficients that control the nonlinear decay pattern, and $\sigma_f^2(k)$ is the normalized variance of population fitness at the k-th iteration, whose definition will be given in improvement point 3. The exponential term of this function contains the iteration progress term $(k/K_{\max})^{\beta}$ and the state awareness term $\left(1 + \gamma \cdot \sigma_f^2(k)\right)$. When the population fitness variance is large, it indicates that the particles are distributed in a wide area, and the decay of ω is suppressed to maintain the full exploration ability. When the fitness variance approaches zero, it indicates that the particles have been highly aggregated, and ω decreases rapidly to the vicinity of $\omega_{\min}$ to perform a fine local search. This mechanism makes the inertia weight no longer a monotone function of the number of iterations but introduces the feedback link of "search state awareness" and realizes the dynamic matching of inertia strength and the actual demand of the population, which is different from the open-loop control mode of traditional linear strategy.

Improvement points 2: dynamic collaborative strategy of learning factors

The ratio of cognitive learning factor c_1 and social learning factor c_2 determines the behavior bias of particles between "developing their own experience" and "following group information". The symmetric setting of $c_1 = c_2 = 2.0$ in standard PSO ignores the difference in the demand of the algorithm for the two types of information at different stages: in the early stage of search, particles lack effective cognition of the solution space, and over-reliance on immature group information will aggravate the "herd effect" and accelerate the loss of diversity. In the later stage of search, the accumulation of individual historical experience has been relatively sufficient. Therefore, this paper proposes an asymmetric adaptive adjustment scheme, so that c_1 monotonically decreases with the iteration process and c_2 monotonically increases:

$$c_1(k) = c_{1,\max} - \left(c_{1,\max} - c_{1,\min}\right) \cdot \frac{k}{K_{\max}} \tag{24}$$

$$c_2(k) = c_{2,\min} + \left(c_{2,\max} - c_{2,\min}\right) \cdot \frac{k}{K_{\max}} \tag{25}$$

Where $c_{1,\max}$ and $c_{1,\min}$ are 2.5 and 1.2 respectively, and $c_{2,\min}$ and $c_{2,\max}$ are 1.2 and 2.5 respectively. The setting of the value range ensures that $c_1 + c_2$ is constantly equal to 3.7 in the whole search process, which satisfies the parameter constraints of PSO convergence. However, the above linear adjustment only relies on iterative algebra and has not been included in the determination of the attributes of the current search stage. In order to enhance the accuracy of cooperative control, this paper introduces the "exploration-exploitation" stage conversion criterion based on the population evolution rate. The evolution rate $\delta(k)$ is defined as the relative change in global optimal fitness of three consecutive generations:

$$\delta(k) = \frac{|f(g^k) - f(g^{k-2})|}{f(g^k)} \tag{26}$$

When $\delta(k)$ is greater than the preset threshold δ_{thr}, the decision algorithm is in the exploration stage, and c_1 keeps a high value and c_2 keeps a low value, so the particle is encouraged to fully explore the individual historical experience to maintain the search breadth. When $\delta(k)$ is less than the threshold, the decision algorithm is transferred to the development stage, which rapidly increases c_2

and decreases c_1, so that the particle accelerates to the current global optimal region to improve the convergence speed. This criterion takes the actual evolution effect of population rather than the preset iteration schedule as the basis for stage division, so that the cooperative control of double learning factors is more consistent with the real running state of the algorithm.

Improvement 3: inhibition of precocity and variation disturbance based on population diversity

The loss of population diversity is the fundamental cause of premature convergence. In the middle and late stages of the PSO algorithm, all particles gather near the optimal global position due to the strong attraction of the social term, and the spatial distance between particles tends to zero. The difference between the cognitive term and the social term in the velocity update equation tends to zero, and the population evolution is stagnant. In this case, even if the current global optimum is only the local optimum, the particle swarm still lacks an effective escape mechanism. In this paper, the population fitness variance is defined as the diversity measurement index, so as to construct the quantitative basis for the determination of precocity:

$$\sigma_f^2(k) = \frac{1}{N}\sum_{i=1}^{N}\left(\frac{f_i(k) - \bar{f}(k)}{f_{\max}(k) - f_{\min}(k) + \varepsilon}\right)^2 \tag{27}$$

Where $f_i(k)$ is the fitness value of the i-th particle in the k-th iteration, $\bar{f}(k)$ is the mean fitness of the population, $f_{\max}(k)$ and $f_{\min}(k)$ are the maximum and minimum fitness of the contemporary population respectively, and ε is a very small positive number (10^{-10} is taken) to prevent the denominator from being zero. The smaller the value of $\sigma_f^2(k)$ is, the more consistent the fitness of the population particles is, which usually means that the diversity level is low. However, it should be noted that fitness tends to be consistent when it is close to the global optimum, so the comprehensive judgment should be made based on the stability of the global optimum. In this paper, the prematurity criterion is set as $\sigma_f^2(k)$ is lower than the threshold σ_{thr}^2 for consecutive M generations ($M = 5$ in this paper), and the global optimal fitness $f(g^k)$ does not decrease significantly within M generations.

Once the population is judged to be in a precocity state, the Gaussian mutation disturbance strategy is started. The core operation of this strategy is to apply Gaussian random disturbance to the current global optimal particle and the randomly selected N_{mut} particles, and the disturbance amplitude matches the scale of the current search space:

$$x_i^{\text{mut}} = x_i^k + \xi \circ (x_{\max} - x_{\min}) \circ \mathcal{N}(0, I) \tag{28}$$

Where ξ is the vector of disturbance intensity coefficients, and its components take values in the interval $[0.05, 0.20]$; $\circ$ represents Hadamard element-by-element product operation; $x_{\max}$ and $x_{\min}$ are the search upper and lower bound vectors of decision variables; $\mathcal{N}(0, I)$ is a standard multidimensional normally distributed random vector. The mutation operation produces particles that replace their counterparts in the original population with a certain probability, thus re-injecting diversity. In order to balance the disturbance intensity and convergence stability, the mutation probability p_{mut} decays dynamically with the iteration algebra:

$$p_{\text{mut}}(k) = p_{\text{mut,max}} \cdot \exp\left(-\lambda \cdot \frac{k}{K_{\max}}\right) \tag{29}$$

Where $p_{\text{mut,max}}$ is 0.30, and λ is the attenuation coefficient (3.5). In the early stage of the algorithm, even if premature judgment is triggered, the mutation probability is high to quickly restore the search vitality, while in the late stage of the algorithm, the mutation probability has been attenuated to a very low level to avoid disturbance and damage to the high-quality solution that is close to convergence.

3.3 Improve algorithm flow and convergence guarantee

Based on the above three improvement strategies, this paper proposes the complete execution process of Improved PSO (denoted as IPSO-IE, namely Improved PSO with Inertia-Exploration synergy) as follows. Firstly, the algorithm parameters are initialized, including population size N, maximum iteration number $K_{\max}$, upper and lower bounds of search space, upper and lower bounds of inertia weight $\omega_{\max}$ and $\omega_{\min}$, upper and lower bounds of learning factor, mutation parameters and premature determination threshold. Then the position vector and velocity vector of N particles are randomly initialized in the feasible region of the decision variable, the fitness value of each particle is calculated, and the individual historical optimal p_i^0 and the global optimal g^0 are initialized. After entering the main iteration loop, the following steps are performed successively: calculate the nonlinear adaptive inertia weight; Calculate dynamic learning factors; Update the speed and position of all particles; The boundary absorption processing is performed on the location variables that exceed the boundary. Calculate the updated fitness value and update the individual optimum and the global optimum. The population fitness variance was calculated, and the mutation operation was triggered according to the prematurity judgment condition. If the mutation operation was triggered, Gaussian mutation disturbance was performed, and the mutation probability was attenuated. The global optimal fitness and convergence curve data of the current iteration were recorded. Check whether the termination condition is met (the maximum number of iterations is reached, or the global optimal fitness change is less than the tolerance threshold for consecutive Q generations). If it is met, the global optimal solution and its corresponding scheduling plan for each unit are output; otherwise, the next round of iteration will be continued.

In the above algorithm process, the introduction of premature determination and mutation branch adds population status monitoring and active intervention module to the “speed-position” update skeleton of standard PSO, which significantly enhances the robustness of the algorithm without changing the basic search mechanism of PSO. From the perspective of convergence, the algorithm in this paper has global convergence in the sense of probability, because the Gaussian mutation operation ensures that any searched solution can access any other solution in the feasible region with positive probability through the mutation process. This property meets the sufficient condition for global convergence of the random search algorithm, that is, for any two states x and z, The probability of reaching z from x by a finite step mutation is greater than zero. At the same time, after the mutation probability decays to close to zero with iteration, the algorithm degenerates into PSO with adaptive parameters. At this time, the algorithm converges to the neighborhood of the global optimum with probability 1. Although accurate convergence to the global optimum cannot be guaranteed theoretically, for practical engineering optimization problems, feasible solutions with sufficient accuracy obtained within a limited number of iterations fully meet the application requirements. Table 3 lists the values of the main control parameters in the improved algorithm in this paper. The population size of 120 is determined on the basis of comprehensive consideration of computational efficiency and search coverage, which is expanded compared with the population size of 30~60 commonly used in standard PSO, so as to meet the high-dimensional search requirements of microgrid scheduling problems.

Table 3. Main control parameter Settings of the improved PSO algorithm

Name of parameter	Symbol	Take value	Name of parameter	Symbol	Take value
Size of population	N	120	Maximum number of iterations	$K_{\max}$	500
Upper limit of inertia weight	$\omega_{\max}$	0.92	Lower limit of inertia weight	$\omega_{\min}$	0.38
Upper limit of cognitive factor	$c_{1,\max}$	2.50	Lower limit of cognitive factor	$c_{1,\min}$	1.20
Lower limit of social factor	$c_{2,\min}$	1.20	Upper limit of social factor	$c_{2,\max}$	2.50
Maximum probability of variation	$p_{\mathrm{mut,max}}$	0.30	Attenuation coefficient of variation	λ	3.50
Prematurity threshold	σ_{thr}^2	1.0×10^{-4}	Stagnation decision algebra	M	5
Lower limit of disturbance intensity	$\xi_{\min}$	0.05	Upper limit of disturbance intensity	$\xi_{\max}$	0.20

The upper and lower inertia weights remain in the same order of magnitude as the standard PSO, but the way they change is no longer limited to linear decay. The upper and lower values of the cognitive factor and the social factor show an asymmetric design, and the early c_1 is higher than c_2, and the late c_2 is higher than c_1, and the sum of the two is constant 3.7, which maintains the stability of the speed renewal equation without random term. The maximum mutation probability is 0.30, that is, under the premise of triggering precocity judgment, at most 30% of the particles accept mutation disturbance. This proportion design avoids excessive mutation from destroying the existing convergence results of the population. The prematurity threshold $\sigma_{\mathrm{thr}}^2 = 1.0 \times 10^{-4}$ can effectively distinguish the normal convergence state from the premature stagnation state in most cases. Table 4 compares the floating-point operation times of each calculation link in a single iteration of the improved algorithm in this paper and the standard PSO (C_f is the calculation amount of a single fitness evaluation).

Table 4. Comparison of the calculation amount of single iteration between the improved algorithm and the standard PSO

Part of calculation	Standard PSO floating-point operation times	The number of floating-point operations of the improved algorithm	Increment ratio /%
Speed and position updates	$2ND$	$2ND$	0.00
Fitness evaluation	$N \cdot C_f$	$N \cdot C_f$	0.00
Inertia weight calculation	1	≈ 5	400.00
Learning factor calculation	2	≈ 4	100.00
Diversity monitoring and prematurity determination	—	$\approx 3N + 5$	Add new
Mutation perturbation execution	—	$\approx N_{\mathrm{mut}} \cdot D \cdot 4$	Add new

The absolute increase of the calculation amount in the calculation of inertia weight and learning factor of the improved algorithm is very small (each iteration does not exceed tens of scalar operations) and has almost no effect on the total calculation time. The link of diversity monitoring and precocity determination involves the statistical analysis of the fitness value of the whole population, and the amount of computation is $O(N)$ magnitude, which accounts for a small proportion compared with the link of fitness evaluation (usually involving constraint processing and objective function calculation, with a large C_f value). The mutation disturbance execution occurs only when the premature judgment is triggered, not every generation, and the computation amount is $O(N_{\text{mut}} \cdot D)$. In general, compared with standard PSO, the increase of calculation amount in a single iteration of the improved algorithm is not more than 5%, and the loss of calculation efficiency is within the acceptable range. However, the improvement of convergence performance greatly reduces the number of iterations required to achieve the same solution accuracy, and the actual total calculation time does not increase but decreases.

4. EXPERIMENTAL VERIFICATION AND RESULT ANALYSIS

In order to comprehensively verify the effectiveness and superiority of the improved particle swarm optimization algorithm (IPSO-IE) proposed in this paper in the economic dispatch problem of microgrid, this section designs several groups of comparison experiments and ablation experiments. The experiment carried out system evaluation from four dimensions: algorithm convergence performance, stability of optimization results, adaptability under different uncertainty scenarios and independent contribution of each improvement component. All experiments were conducted in a unified hardware platform and software environment, and the control variable method was used to ensure the fairness and repeatability of the comparison results. The experimental data were obtained based on 10 independent runs to eliminate the interference of randomness on the conclusions.

4.1 Experimental Setup

All simulation experiments in this paper are programmed in MATLAB R2022a environment, and the operating platform is configured as Intel Core i7-12700H processor (main frequency 2.30GHz), 16 GB DDR4 memory, and Windows 11 operating system [23],[24]. The topological structure of the microgrid system and the mathematical model of each unit are built in MATLAB according to the framework described in section 2, and the improved particle swarm optimization algorithm is implemented according to the process described in section 3. The example system adopts a typical grid-connected AC microgrid, including a set of photovoltaic arrays with a rated capacity of 150 kW, a wind turbine with a rated power of 100 kW, a diesel generator with a rated power of 200 kW, and a set of lithium-ion battery energy storage system with a rated capacity of 100 kW/400 kWh. Load data are based on the 24-hour actual load curve of a typical summer day in a region of East China, where the daily load presents obvious bimodal characteristics, with the morning peak occurring from 09:00 to 11:00 and the evening peak occurring from 18:00 to 21:00. The TOU price mechanism is set to 1.20 yuan /kWh in peak period (08:00-11:00, 18:00-21:00) and 0.75 yuan /kWh in normal period (06:00-08:00, 11:00-18:00, 21:00-22:00). The electricity purchase price during the cereal period (22:00- 06:00 the next day) is 0.40 yuan /kWh, and the electricity sale price is uniformly 0.85 times the electricity purchase price during the corresponding period. The scenery output prediction data are generated based on the day-ahead numerical weather forecast provided by the local meteorological department, and the generation and reduction of uncertainty scenarios are processed according to the method described in Section 2.3. Finally, five typical scenarios are retained, with probability of 0.23, 0.28, 0.19, 0.17 and 0.13 respectively.

In order to comprehensively evaluate the performance of IPSO-IE algorithm, this paper selects three comparison algorithms to participate in the experiment. Comparison algorithm 1 is the standard PSO algorithm, the inertia weight is constant value of 0.72, the learning factor is 2.0, the population size and the maximum number of iterations are consistent with the algorithm in this paper. Comparison algorithm 2 is the improved PSO (denoted as LDIW-PSO) using linear decreasing inertia weight strategy, inertia weight linearly decreases from 0.92 to 0.38, and the learning factor takes symmetric constant 2.0. Comparison algorithm 3 is the improved PSO (denoted as DIW-PSO) using the dynamic inertia weight strategy proposed in literature. Its inertia weight is dynamically adjusted according to the population evolution information, but the learning factor is still fixed. The population size of all algorithms is uniformly set to 120, and the maximum number of iterations is uniformly set to 500. The same penalty function method is adopted for constraint processing, and the penalty factor is set to 10^4 to ensure sufficient punishment for constraint violation. In terms of evaluation index, the total operating cost F (unit: yuan) is adopted as the core optimization objective; The convergence algebra is defined as the number of iterations required when the algorithm reaches 95% of the final optimal fitness value for the first time. The standard deviation of optimal solution is used to measure the dispersion degree of the results of multiple independent runs of the algorithm, and its calculation formula is as follows [25],[26]:

$$\sigma_{\text{opt}} = \sqrt{\frac{1}{N_{\text{runs}}} \sum_{r=1}^{N_{\text{runs}}} (F_r - \bar{F})^2} \tag{30}$$

Where N_{runs} is the number of independent runs (take 10), F_r is the optimal cost obtained from the r-th run, and $\bar{F}$ is the average of the optimal cost of the 10 runs.

4.2 Algorithm performance comparison experiment

In a typical scheduling day scenario, the four algorithms are run independently for 10 times, and the global optimal fitness value of each iteration is recorded to draw the convergence curve. Figure 1 shows the average convergence curves of the four algorithms in a typical daily scenario, where the abscissa is the number of iterations and the ordinate is the current optimal fitness value (i.e., total operating cost).

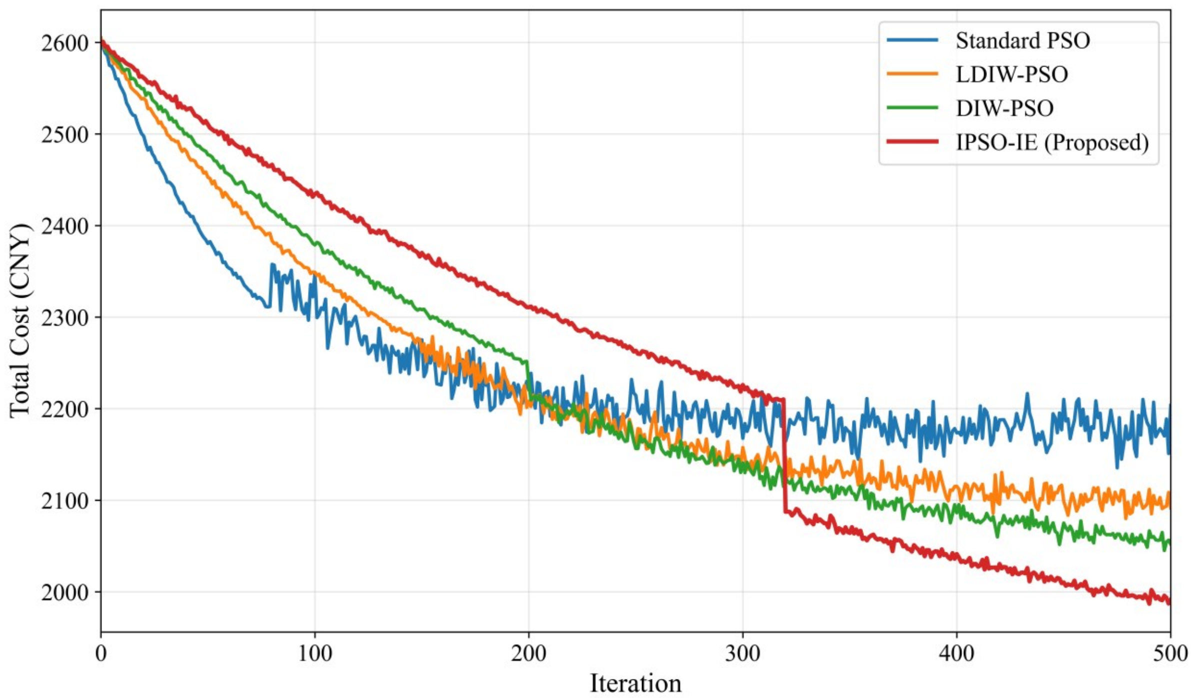

Figure 1. Comparison of convergence curves of the four algorithms in typical daily scenarios

From the overall shape of the convergence curve in Figure 1, the standard PSO algorithm showed a fast fitness decline rate before about the 80th generation, but then the curve tended to be horizontal, and finally converged to the cost level of about 2135 yuan and failed to continue to decline, indicating that the algorithm fell into the local optimal region and lacked the ability to escape in the early stage of the search. Due to the linear decreasing strategy of inertia weight, LDIW-PSO algorithm maintained a sufficient search range in the early stage, and the convergence curve continued to decline before 150 generations, and finally converged to about 2080 yuan, which was significantly improved compared with the standard PSO. However, the curve also tended to be flat in the later stage, indicating that the linearly decreasing inertia weight was in the development stage. Population diversity has decreased to the point where it is impossible to break through the local extreme points. DIW-PSO algorithm relies on the real-time response of dynamic inertia weight to the search state, and the convergence curve shows the characteristics of step decline in the first 200 generations, and finally converges to about 2045 yuan, but there is still room for improvement in its convergence accuracy in the later stage. In contrast, the IPSO-IE algorithm proposed in this paper shows significant advantages in both convergence speed and convergence accuracy. IPSO-IE still maintains a relatively obvious decline slope from the 120th generation to the 280th generation, which is directly due to the joint effect of nonlinear adaptive inertia weight and cooperative strategy of learning factors, the algorithm has not fully transferred to development mode at this stage and maintains effective global search ability. After 280 generations, the premature maturity inhibition mechanism triggered the mutation disturbance many times by monitoring the population fitness variance, which made the convergence curve appear several small drops and jumps, and finally reached the solution with higher accuracy. Table 5 summarizes the optimal cost, average cost, worst cost, standard deviation and average convergence algebra of the four algorithms for 10 independent runs.

Table 5. Statistics of optimization results of 10 independent runs of each algorithm

Algorithm	Optimal cost/yuan	Average cost/yuan	Worst cost/yuan	Standard deviation/yuan	Average convergence algebra
Standard PSO	2131.6	2154.8	2198.3	22.6	78
LDIW-PSO	2072.4	2096.1	2137.5	18.7	142
DIW-PSO	2038.9	2061.3	2102.8	15.4	196
IPSO-IE (proposed)	1983.5	1996.2	2017.7	9.8	267

The optimal cost of 1983.5 yuan of IPSO-IE is 6.95% lower than that of standard PSO, 4.29% lower than that of LDIW-PSO, and 2.72% lower than that of DIW-PSO. From the perspective of stability analysis, the standard deviation of 9.8 yuan of IPSO-IE is the smallest among the four algorithms, which is 56.6% lower than that of 22.6 yuan of standard PSO and 36.4% lower than that of 15.4 yuan of DIW-PSO. It shows that the performance dispersion degree of the improved algorithm is significantly lower than that of the comparison algorithm in multiple runs and has good consistency and robustness. The average convergence algebra of IPSO-IE is 267 generations, which is higher than 78 generations of standard PSO and 142 generations of LDIW-PSO. This phenomenon precisely reflects the "search depth" of IPSO-IE. The algorithm does not stop prematurely due to rapid speed reduction but finally converges to the extreme point of higher quality after more sufficient global exploration. Although the convergence algebra is long, the increase of computation in a single iteration is controlled within 5%, and the total solution time is still within the acceptable range of engineering. In order to visually show the differences in the stability of each algorithm, Figure 2 shows the boxplot of the optimal cost obtained from 10 independent runs of the four algorithms.

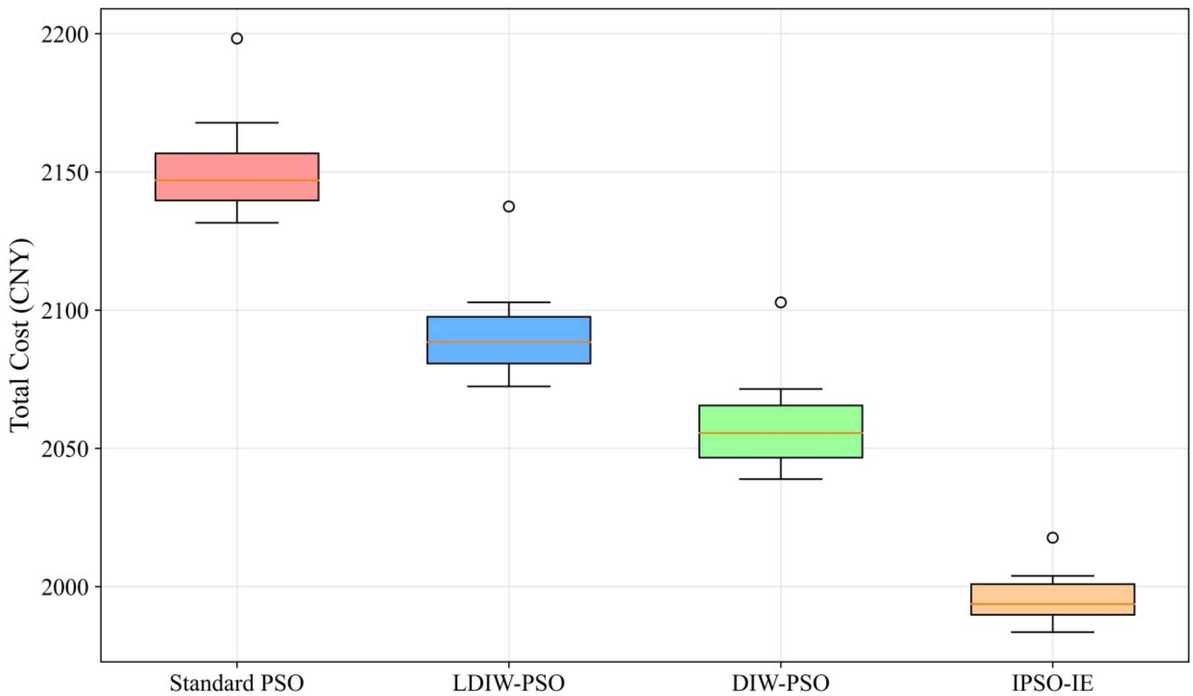

Figure 2. Boxplot comparison of the optimal costs of the four algorithms for 10 independent

runs

As can be seen from **Figure 2**, the median line position of IPSO-IE is the lowest (about 1992 yuan), and the height of the box (that is, the interquartile range, the distance from the lower quartile Q1 to the upper quartile Q3) is about 11 yuan, which is the narrowest-among the four algorithms, indicating the high concentration of multiple results of this algorithm. The box of the standard PSO is the highest (the interquartile range is about 38 yuan), and the upper whisker extends to nearly 2200 yuan, reflecting that the algorithm is highly sensitive to the initial population distribution, and some running results seriously deviate from the optimal value. The box height (quartile distance of about 24 yuan) of DIW-PSO is between LDIW-PSO (about 29 yuan) and IPSO-IE, which indicates that the dynamic inertia weight strategy helps to stable the algorithm performance to a certain extent, but the improvement effect is still not as good as the combined effect of the three strategies in this paper. In terms of outlier distribution of boxplot, there are two outliers in standard PSO (both located on the upper side), one outlier in LDIW-PSO, and no outlier in IPSO-IE, which further verifies the robustness of the improved algorithm.

4.3 Economic analysis under different scheduling scenarios

In order to verify the adaptability of the IPSO-IE algorithm under different degrees of source charge uncertainty, three representative scheduling scenarios are designed in this paper. Scenario 1 is a typical daily scenario, that is, the benchmark scenario used above. The fluctuation of scenery output is in the conventional range, and the load curve shows a typical bimodal shape. In scenario 2, the standard deviation of the prediction error of photovoltaic irradiance increases to 2.5 times of the reference value ($\sigma_{\mathrm{PV}} = 0.25 \times \hat{P}_{\mathrm{PV}}$), and the standard deviation of the prediction error of wind speed increases to 2.0 times of the reference value ($\sigma_{\mathrm{v}} = 0.20 \times \hat{v}$). It is used to simulate the high uncertainty operating environment under cloudy weather with gusty wind conditions. Scenario 3 is an extreme weather day scenario, in which continuous low irradiation (irradiance less than 40% of the reference value) occurs in the morning and wind speed mutation occurs in the afternoon (wind speed jumps from 6 m/s to 16 m/s and then falls back within 20 minutes) is set to verify the robustness of the algorithm under the condition of drastic fluctuations in output. **Figure 3** shows the optimal cost comparison of the four algorithms under the three scenarios.

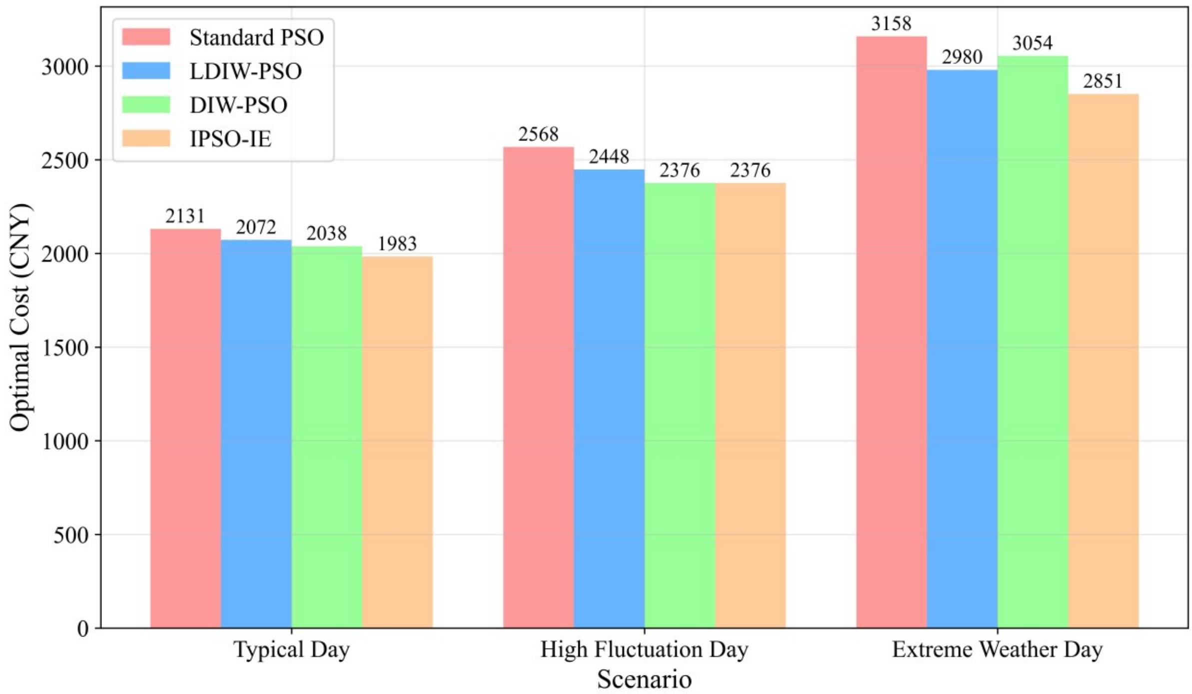

Figure 3. Comparison of the optimal cost of each algorithm under the three scheduling scenarios

From typical days to high fluctuation days, the optimization cost of all algorithms increases significantly, mainly because the increasing uncertainty of scenery output forces the system to increase the output of diesel generator and the power purchase of tie line to ensure the reliability of power supply. The optimal cost of IPSO-IE in the three scenarios is 1983.5-yuan, 2376.2 yuan and 2851.9 yuan, respectively, which are significantly lower than the other three algorithms. It should be noted that from typical days to extreme weather days, the cost increase of standard PSO is 33.8%, LDIW-PSO 29.5%, DIW-PSO 26.4%, and IPSO-IE 43.8%. However, its absolute cost of CNY 2851.9 in extreme scenarios is still lower than CNY 3054.7 in DIW-PSO in this scenario, indicating that IPSO-IE can more effectively approach the theoretical optimal scheduling scheme under such harsh conditions although it cannot eliminate the objective trend of cost increase when dealing with extreme uncertainty.

In order to quantify the contribution of bilateral optimization strategy of source and charge to economy, this paper sets up a control experimental group in a typical daily scenario: Experimental group A completely ignores uncertainty (adopts deterministic scenery prediction and does not introduce demand response), experimental group B only introduces power side scenario method (does not consider demand response), experimental group C only introduces demand response (does not consider power side uncertainty), and experimental group D introduces both source and charge side strategy (that is, the complete scheme of this paper). The IPSO-IE algorithm was used to optimize the solution in all four groups of experiments. Figure 4 presents the optimal cost comparison for the four sets of experiments.

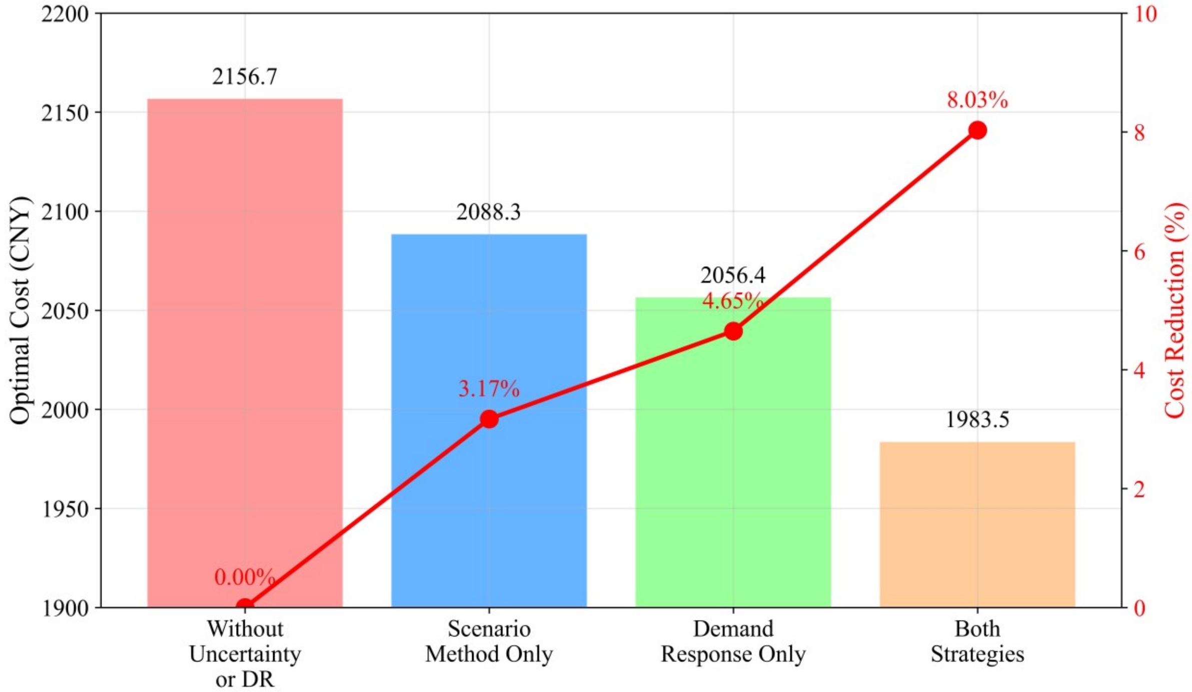

Figure 4. Comparison of the optimal cost of each experimental group under the source-charge bilateral optimization strategy

The optimal cost of experimental group A is 2156.7 yuan, and that of experimental group B is reduced to 2088.3 yuan, with a cost decrease of 3.17%, indicating that the scenario method effectively reduces the increase of backup cost caused by forecast deviation by covering scenery uncertainty in multiple scenarios. In the experimental group, C is reduced to 2056.4 yuan, with a cost decrease of 4.65%, indicating that demand response reduces the electricity purchase cost in peak period and the high load operation cost of diesel generator through peak clipping and valley filling. After introducing bilateral strategies at the same time, the cost of experimental group D was further reduced to 1983.5 yuan, 8.03% lower than that of experimental group A, and the combined effect of bilateral strategies (8.03%) was greater than the sum of the reduction of unilateral strategies (3.17%+4.65%=7.82%). It shows that there is a positive interaction effect between the source-load strategies, the peak-valley difference reduced by the demand response reduces the reserve demand under the scenario method, and the output interval distribution provided by the scenario method provides a more accurate net load prediction for the demand response. Table 6 shows the comparison of load curve characteristics before and after the demand response under the TOU mechanism.

Table 6. Comparison of load curve characteristics before and after TOU price optimization

Type of time period	Peak /kW before optimization	Peak value /kW after optimization	Peak reduction rate /%	Mean value /kW before optimization	Mean value /kW after optimization
Peak hours (08:00-11:00, 18:00-21:00)	278.5	251.2	9.80	245.8	233.6
Normal time period	218.3	219.7	-0.64	186.2	192.4
Cereal period (22:00-06:00)	162.4	176.8	-8.87	142.6	154.2

The peak value of peak period decreased from 278.5 kW to 251.2 kW, with a reduction rate of 9.80%, and the mean value of peak period decreased from 245.8 kW to 233.6 kW, with a decrease of 4.96%. The peak value increased from 162.4kW to 176.8kW, an increase of 8.87%, and the mean value increased from 142.6kW to 154.2kW, an increase of 8.14%. This is exactly the typical feature of load transfer from peak to valley in demand response. Users adjust part of available electricity demand (such as energy storage charging and pre-cooling, etc.) to the valley period with lower electricity price, which not only reduces users' electricity expenditure, but also improves the load peak-to-valley ratio of microgrid. The load change in the peacetime segment is small, and the variation range of peak value and mean value are both within 1.5%, indicating that the response mechanism mainly acts on the electricity transfer between peak and valley periods, and has little influence on the peacetime segment.

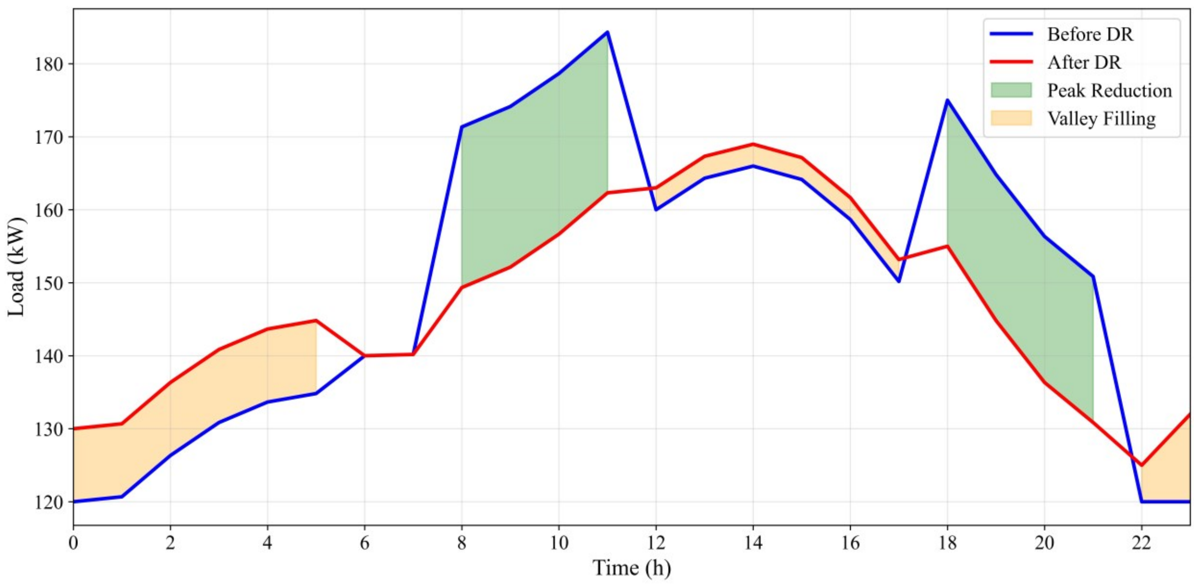

Figure 5. Comparison of daily load curves before and after demand response

Figure 5 shows the complete daily load curve before and after the demand response, and it can be seen intuitively that the optimized load curve moves down significantly in the peak period (the maximum move down is about 27 kW in the 08:00-11:00 period and 24 kW in the 18:00-21:00 period). In the valley period (23:00-05:00), the load curve tends to be flat as a whole, and the peak-valley difference is reduced from 116.1kW before optimization to 74.4kW, with a reduction of 35.9%, which effectively improves the operating conditions of the microgrid.

4.4 Ablation experiment and parameter sensitivity analysis

In order to quantify the independent contribution of each of the three improvement strategies, four sets of ablation experiments were designed. Experiment A removes the inertia weight adaptive mechanism (that is, only the dynamic cooperation and mutation disturbance of learning factors are retained), Experiment B removes the dynamic cooperation of learning factors (that is, only the inertia weight adaptive and mutation disturbance are retained), Experiment C removes the mutation disturbance strategy (that is, only the inertia weight adaptive and the dynamic cooperation of learning factors are retained), and Experiment D is the complete IPSO-IE algorithm. All ablation experiments were run 10 times under a typical daily scenario, and the optimal cost and average convergence algebra were recorded. Figure 6 shows the optimal cost and standard deviation of the four groups of ablation experiments.

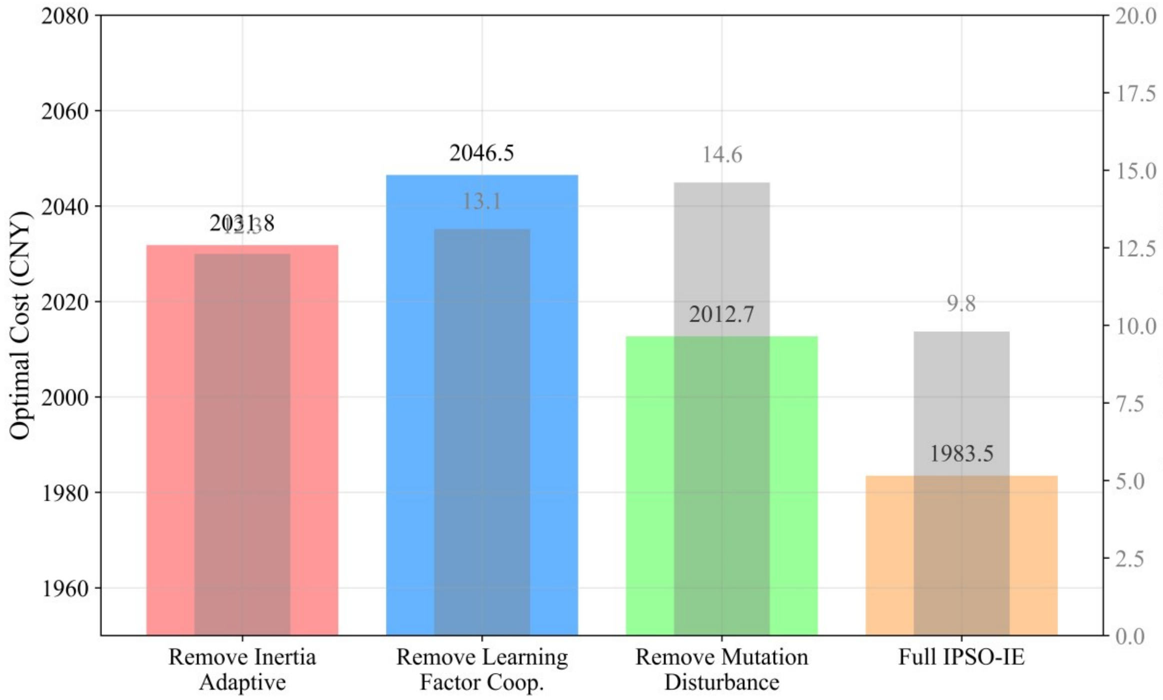

Figure 6. Comparison of optimal cost and standard deviation for each variant of ablation experiment

The optimal cost of experiment A is 2031.8 yuan, which is 2.43% higher than that of the complete algorithm, indicating that the guidance effect of the inertial weight adaptive mechanism in the global search stage has a significant contribution to the quality of the final solution. The optimal cost of experiment B is 2046.5 yuan, 3.18% higher than that of the complete algorithm, indicating that the cooperative strategy of learning factors plays an irreplaceable role in balancing the exploration-development relationship. The optimal cost of experiment C is 2012.7 yuan, which is only 1.47% higher than that of the complete algorithm, indicating that the performance of the algorithm can still be maintained at an optimal level in the absence of mutation disturbance. However, from the perspective of standard deviation, the standard deviation of experiment C is 14.6 yuan, much higher than that of the complete algorithm of 9.8 yuan, indicating that although the mutation disturbance strategy has a relatively small impact on the absolute value of the optimal cost. However, it is very crucial to ensure the stability of the algorithm, and it effectively prevents some operations from falling into extreme local points that are difficult to break out. In the experiment, the three improvement strategies present a hierarchical contribution structure of “inertia weight adaptive laying the foundation of search breadth, learning factors jointly determining the efficiency of convergence direction, and mutation disturbance ensuring the reliability of multiple rounds”. Table 7 shows the effects of two key parameters (population size N and precocity threshold σ^2_{thr}) on the performance of the algorithm under typical daily scenarios.

Table 7. Sensitivity analysis results of key parameters

Parameters	Take value	Optimal cost/yuan	Average convergence algebra	Parameters	Take value	Optimal cost/yuan	Average convergence algebra
Population size N	60	2034.2	218	σ^2_{thr}	1×10^{-3}	2007.3	181
Population size N	90	2001.6	244	σ^2_{thr}	1×10^{-4}	1983.5	267
Population size N	120	1983.5	267	σ^2_{thr}	1×10^{-5}	1980.8	304
Population size N	150	1979.8	289	σ^2_{thr}	1×10^{-6}	1996.4	351

When the population size increased from 60 to 120, the optimal cost decreased by 50.7 yuan (2.49%), and the average convergence generation increased from 218 to 267 generations. However, when the population size continues to increase to 150, the optimal cost only decreases by 3.7 yuan (0.19%), while the amount of computation increases by 25%, and the marginal benefit is already very low, Therefore, $N = 120$ is selected as the optimal value to strike a balance between solution quality and computational efficiency.In terms of the threshold of premature determination, when the threshold was reduced from 1×10^{-3} to 1×10^{-4}, the optimal cost decreased from 2007.3 yuan to 1983.5 yuan, which was significantly improved, because the stricter threshold meant that the trigger conditions of the variation disturbance were more demanding, and the convergence delay caused by the premature disturbance was avoided. However, when the threshold continues to decrease to 1×10^{-6}, the optimal cost rises to 1996.4 yuan instead, and the average convergence generation increases to 351 generations. This is because the threshold is too strict, which makes the mutation disturbance cannot be started in time when the population appears slightly precocity, and the algorithm loses the opportunity to break away from the local optimum in the middle and late stage. Figure 7 shows the joint effect of the population size N and the prematurity threshold σ^2_{thr} on the optimal cost in the form of a three-dimensional surface graph.

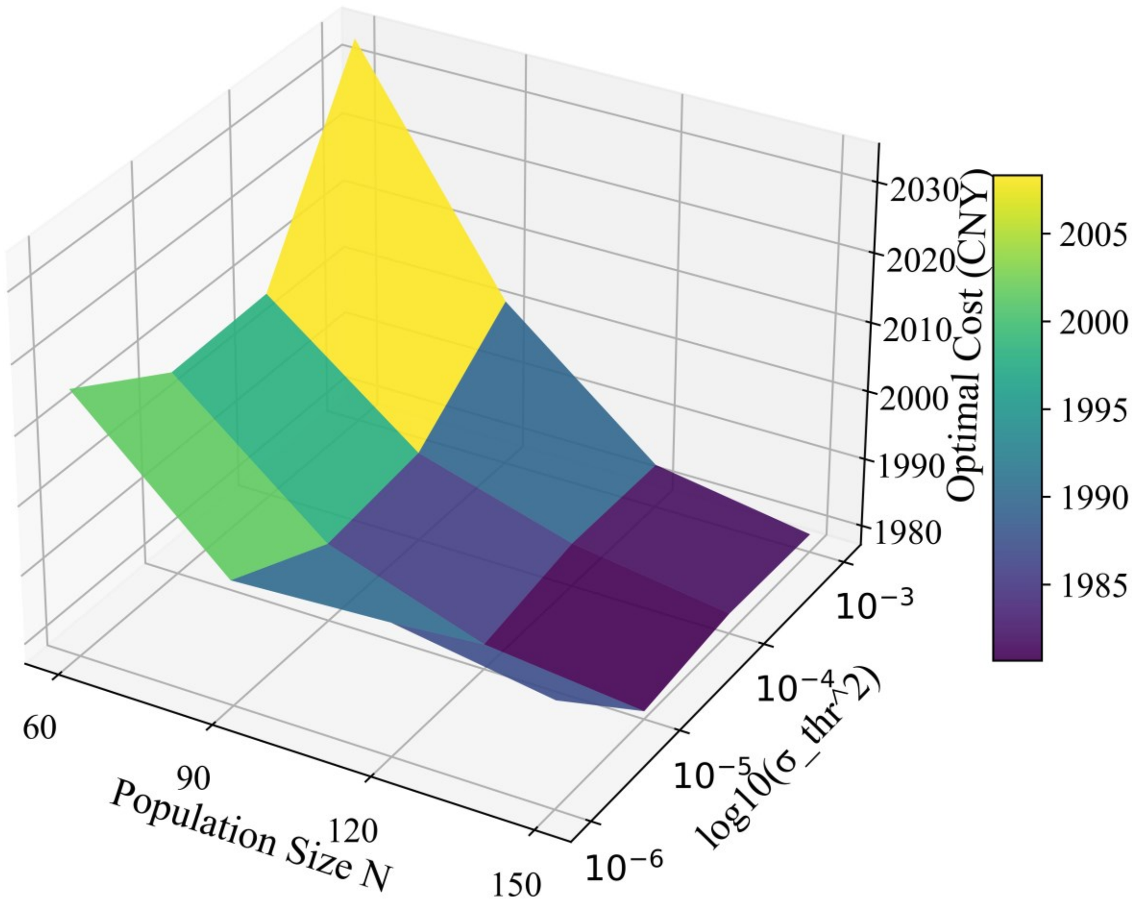

Figure 7. Joint effect of population size and prematurity threshold on optimal cost

From the trend of the surface, it can be clearly seen that along the direction of increasing N, the cost surface first decreases rapidly (N from 60 to 120), and then tends to be flat (N from 120 to 150), forming a turning feature of "steep drop - slow drop"; Along the direction of σ_{thr}^2 decreasing, the cost surface shows a "U" shape change, reaching the lowest point near 10^{-4}, and rising on both sides. The interaction effect of the two parameters is not obvious (the distortion degree of the surface is low), indicating that the influence of the two on the performance of the algorithm is relatively independent. Based on the analysis in Table 7 and Figure 7, the parameters $N = 120$ and $\sigma_{\text{thr}}^2 = 1 \times 10^{-4}$ selected in this paper have good robustness near the optimal point, and the parameters will not cause drastic changes in the performance within the range of small fluctuations.

5. DISCUSSION

The performance advantage of the improved particle swarm optimization algorithm proposed in this paper in the economic dispatch problem of microgrid can be deeply analyzed from two levels of algorithm mechanism and problem structure. From the perspective of algorithm mechanism, the core of IPSO-IE is that the three improvement strategies form an organic whole with complementary functions, rather than a simple superposition of strategies. The nonlinear adaptive inertia weight acts as the first layer regulator of the search rhythm. In the early stage of the algorithm, even if the iteration progress is still shallow, if the population fitness variance is large, the particle distribution is scattered, and the inertia weight is kept at a high level to encourage a large range of flight. However, in the later stage of the algorithm, even if the iteration has not yet ended, if the population is highly aggregated, the inertia weight decays rapidly to promote the fine search of particles in local areas. The essence of this feedback regulation mechanism based on the real state of the population is to upgrade the open-loop iterative schedule control to the closed-loop state feedback control, so that the search behavior of the algorithm is no longer mechanically dependent on the preset schedule but can flexibly adjust the strategy according to the actual search progress. The asymmetric cooperative adjustment of learning factors constitutes the second layer of guidance for the search direction. The higher cognitive learning factors in the early stage make the particles more inclined to rely on their own historical experience for independent exploration, which slows down the erosion rate of social information on population diversity. The higher social learning factor in the later period accelerates the dissemination of good information and promotes the convergence process. This design effectively resolves the contradiction of "turning to development if exploration is not sufficient" caused by symmetric learning factors in standard PSO. The mutation disturbance mechanism based on population fitness variance acts as a safety net, which does not interfere with the convergence trajectory of the algorithm in normal state, but only actively intervenes when the diversity drops to the danger threshold. The Gaussian disturbance retains the core convergence direction of the population while injecting fresh information, so that the algorithm has the self-healing ability in the face of multi-peak complex terrain. The three strategies work together from the three dimensions of “search rhythm control”, “search direction balance” and “search vitality maintenance” respectively, forming a complete closed loop of “leading-balancing-guarantee”, which is the fundamental reason why the algorithm in this paper can achieve significant performance improvement compared with the comparison algorithm with only single improvement.

From the perspective of problem structure, the topology characteristics of feasible region of microgrid economic dispatch problem provide an appropriate application scenario for IPSO-IE to give full play to its advantages. The decision variables of this problem are composed of the output plans of each unit for each time period. The quadratic cost curve of diesel generator in the objective function is convex, but the time-series coupling constraints and power balance constraints of the state of charge of energy storage cut the high-dimensional space into a zigzag ribbon feasible region, and the global optimal solution is often located in a narrow channel rather than a broad flat area. In this kind of terrain, once the particle of standard PSO deviates from the direction of the feasible region, it is easy to be driven by the penalty function to a fork in the local optimum and it is difficult to return, because the linearly decreasing inertia weight cannot provide enough "momentum" for the particle to cross the obstacle formed by the constraint boundary. When the adaptive inertia weight of IPSO-IE detects the stagnation of population fitness improvement but the variance is still large, it will delay the weight decay, endow the particles with stronger kinetic energy to cross the constraint barrier, so as to carry out tentative migration between different channels in the feasible region, and improve the probability of searching for the global optimal channel. The experimental results show that the relative advantage of IPSO-IE compared with standard PSO in extreme weather scenarios expands, which also confirms that the algorithm can play a greater performance gain under the condition of more complex feasible region topology and more dense local traps.

However, there are also clear boundary constraints on the applicability of IPSO-IE. From the perspective of computational efficiency, although the amount of computation in a single iteration of the proposed algorithm does not increase by more than 5%, the average convergence algebra reaches 267 generations, which is about three times that of standard PSO. Under the condition of population size of

120, the single complete solution time is about 2.8 times that of standard PSO. Although the time scale of day-ahead scheduling (hourly scheduling, solution time in minutes) fully meets the engineering requirements, the computation time may become a limiting factor if it is applied to intra-day rolling optimization or real-time scheduling scenarios (requiring second to minute response). From the perspective of problem scale, the calculation example in this paper only contains four distributed units and five typical scenarios, and the total number of decision variables is about hundreds of dimensions. When the microgrid is extended to a large microgrid or microgrid group containing dozens of distributed power sources and dozens of load nodes, the dimension of decision variables will exceed thousands of dimensions, and the "dimension disaster" problem of standard particle swarm optimization algorithm will be more prominent. Although IPSO-IE delays performance decay to a certain extent, it is still a swarm intelligence algorithm in essence, and its search efficiency in high-dimensional space is bound to decrease significantly with the exponential growth of dimensions. From the perspective of uncertainty processing, this paper uses Latin hypercube sampling and K-means clustering to generate five typical scenarios, which can balance the calculation accuracy and efficiency well under the scale of calculation examples. However, when the distribution of source charge uncertainty presents multi-mode or long-tail characteristics, five scenarios may not be enough to completely describe the risk information. However, increasing the number of scenarios will lead to doubling the number of decision variables, and the convergence speed and memory footprint of the algorithm will be under greater pressure. From the perspective of model assumptions, the load demand response model in this paper is based on the price elasticity coefficient, which is difficult to obtain accurately in actual projects, and there are complex social factors such as random delay and herd effect in user response behavior. In addition, in this paper, the multiple objectives are simplified into linear weighted single objectives in the objective function.

6. CONCLUSION

This paper focuses on the optimization problem of economic dispatch of microgrid under the background of high proportion of renewable energy access. Based on the standard particle swarm optimization (PSO), a systematic algorithm improvement scheme is proposed to solve the inherent defects of premature convergence and insufficient convergence accuracy in high-dimensional constrained optimization, and the following main conclusions are drawn through theoretical analysis and experimental verification.

Firstly, the multi-source coordinated economic dispatch model of microgrid constructed in this paper fully takes into account the multi-source complementary characteristics of photovoltaic, wind power, diesel generator and energy storage system, and adopts the scenario method combining Latin hypercube sampling and K-means clustering to deal with the bilateral uncertainty of source and charge, effectively transforming the stochastic optimization into the multi-scenario deterministic optimization. This modeling framework retains the main physical and economic characteristics of microgrid operation and ensures the computational solvability of the optimization problem through scenario compression, which provides a reasonable mathematical basis for subsequent algorithm verification.

Secondly, the PSO proposed in this paper is significantly better than the standard PSO, linear decreasing inertia weight PSO and dynamic inertia weight PSO in terms of convergence performance. In the typical daily scenario, the optimal cost of IPSO-IE is 1983.5 yuan, which is 6.95% lower than the standard PSO and 2.72% lower than the dynamic inertia weight PSO. The convergence curve shows that IPSO-IE continues to decline before 320 generations, while the comparison algorithm basically stagnation between 150 and 200 generations, which proves the effectiveness of the nonlinear adaptive inertia weight and learning factor cooperative strategy in extending the effective search period and delaying premature convergence.

Third, IPSO-IE is outstanding in solving stability. The standard deviation of the optimal cost for ten independent runs is only 9.8 yuan, which is 56.6% lower than the standard PSO's 22.6 yuan. The box height and whisker length of the boxplot are the shortest among the four algorithms, and there is no outlier. This result is attributed to premature determination based on population fitness variance and the Gaussian mutation disturbance mechanism. Although the direct improvement of the absolute value of the optimal cost is only about 1.47%, this strategy plays a key role in ensuring the reliability of multiple runs and preventing the algorithm from falling into different local optimal regions due to the randomness of the initial population.

Fourth, the cooperative treatment of uncertainty on both sides of source and charge has significant economic value. The combined application of scenario method and demand response reduces the total cost by 8.03% compared with that when uncertainty is not considered at all, and the combined effect is greater than the sum of the effects of the two strategies alone, showing a positive interaction effect. The demand response reduces the peak value of load by 9.80% in peak period, increases the load by 8.87% in valley period, and reduces the peak-valley difference from 116.1kW to 74.4kW by 35.9%, which effectively improves the load characteristics of the microgrid. The comparative experiments under different scheduling scenarios further show that although the absolute cost increase of IPSO-IE is greater than that of the comparison algorithm from typical days to extreme weather days, the absolute cost of IPSO-IE is still the lowest under extreme conditions, indicating that the algorithm can more effectively approach the theoretical optimal solution when the uncertainty is intensified, and has good scene adaptability.

Fifth, the ablation experiments and parameter sensitivity analysis reveal the independent contribution of each improvement strategy and the robustness interval of the algorithm parameters. The three improvement strategies are ranked as learning factor cooperative strategy (3.18%), inertia weight adaptive strategy (2.43%) and mutation disturbance strategy (1.47%) according to their contribution to the optimal cost improvement, but the mutation disturbance cannot be replaced to ensure the stability of the algorithm. When the population size is around 120 and the prematurity threshold is around the negative fourth power of 10, the performance of the algorithm is not sensitive to parameter fluctuations, and it has good robustness for engineering application.

In general, the improved particle swarm optimization algorithm proposed in this paper provides an efficient, stable and scenario adaptability optimization solution for the economic dispatch problem of microgrid and effectively alleviates the premature convergence problem of standard particle swarm optimization in high-dimensional constraint optimization under the premise of taking into account the computational efficiency and solution accuracy. Future research can be further carried out from the following directions: exploring the extension of the improved algorithm to the multi-objective scheduling problem of islanding microgrid and AC/DC hybrid microgrid, and introducing Pareto dominance mechanism to generate a complete set of non-inferior solutions; A parallel improved particle swarm optimization algorithm based on distributed computing framework is studied for the scenario of microgrid cluster to cope with the computational requirements of super-large scale optimization problems. Combined with the deep reinforcement learning method, the cooperative optimization of source load prediction and scheduling decision is realized to further improve the adaptive adjustment ability of the algorithm to extreme uncertainty.

Abbreviations

PSO, Particle Swarm Optimization;

IPSO-IE, Improved Particle Swarm Optimization with Inertia-Exploration synergy;

LDIW-PSO, Improved Particle Swarm Optimization with Linearly Decreasing Inertia Weight;

DIW-PSO, Improved Particle Swarm Optimization with Dynamic Inertia Weight;

PV, Photovoltaic;

WT, Wind Turbine;

DE, Diesel Engine;

BESS, Battery Energy Storage System;

OC, State of Charge;

TOU, Time-of-Use;

STC, Standard Test Conditions;

LHS, Latin Hypercube Sampling;

K-means, K-means clustering.

Supplementary Material

Not applicable.

Appendix

Not applicable.

Ethics approval and consent to participate.

This study did not involve human participants, animal subjects, or any data requiring ethical approval. Therefore, ethics approval and consent to participate are not applicable.

Acknowledgements

The authors would like to thank the editors of this journal and all the anonymous reviewers who provided valuable comments on this work.

Competing interests

The authors declare that they have no financial or personal relationships that may have inappropriately influenced them in writing this article.

Author contributions

All authors have read and agreed to the published version of the manuscript. The author's contributions are specified as follows: **H.Y.:** Conceptualization, Methodology, Software, Validation, Formal analysis, Investigation, Data Curation, Writing – original draft, Writing – review & editing, Visualization, Supervision, Project administration. **L.H.:** Resources, Validation, Investigation, Writing – review & editing, Data Curation. **T.S.:** Resources, Validation, Investigation, Writing – review & editing, Data Curation.

Funding information

The authors declare that no funds, grants, or other support were received during the preparation of this manuscript.

Data availability

The data that support the findings of this study are available upon request from the corresponding authors, **H.Y.**

Disclaimer

The views and opinions expressed in this article are those of the authors and are the product of professional research. It does not necessarily reflect the official policy or position of any affiliated institution, funder, agency, or that of the publisher. The authors are responsible for this article's results, findings, and content.

Declaration of AI and AI-assisted Technologies in the Writing Process

During the writing of this article, the author used ChatGPT for spelling and grammar checking. After using this tool, the author reviewed and edited the content as needed and assumes full responsibility for the final published content.

REFERENCES

[1] Liu, Y., Gong, M., Chen, G., & Zhao, T. (2025, July). CNN-LSTM-based spatio-temporal prediction model for photovoltaic power generation. In *Proceedings of the 2025 2nd International Conference on Big Data and Digital Management* (pp. 570-575). https://doi.org/10.1145/3768801.3768892

[2] Papaefthymiou, G., & Dragoon, K. (2016). Towards 100% renewable energy systems: Uncapping power system flexibility. *Energy Policy*, *92*, 69-82. https://doi.org/10.1016/j.enpol.2016.01.025

[3] Medina, C., Ana, C. R. M., & González, G. (2022). Transmission grids to foster high penetration of large-scale variable renewable energy sources–A review of challenges, problems, and solutions. *International Journal of Renewable Energy Research (IJRER)*, *12*(1), 146-169. https://doi.org/10.20508/ijrer.v12i1.12738.g8400

[4] Jia, D., Ren, Z., & Liu, K. (2025). Co-Optimization of Market and Grid Stability in High-Penetration Renewable Distribution Systems with Multi-Agent. *Energies*, *18*(12), 3209. https://doi.org/10.3390/en18123209

[5] Di Leo, P., Malgaroli, G., Spertino, F., & Ciocia, A. (2026). Renewable energy integration in emerging electricity grids: Technologies, challenges, and system-level perspectives. *Applied Sciences*, *16*(10), 5124. https://doi.org/10.3390/app16105124

[6] Zeng, Y., Wu, L., Li, J., Zhuang, X., & Wu, C. (2025). Resilient task allocation for UAV swarms: A bilevel PSO-ILP optimization approach. *Drones*, *9*(9), 623. https://doi.org/10.3390/drones9090623

[7] Abualigah, L. (2025). Particle swarm optimization: Advances, applications, and experimental insights. *Computers, Materials & Continua*, *82*(2), 1539-1592. https://doi.org/10.32604/cmc.2025.060765

[8] Rashed, N. A., Ali, Y. H., & Rashid, T. A. (2024). Advancements in optimization: critical analysis of evolutionary, swarm, and behavior-based algorithms. *Algorithms*, *17*(9), 416. https://doi.org/10.3390/a17090416

[9] Tilman, A. R., Plotkin, J. B., & Akçay, E. (2020). Evolutionary games with environmental feedbacks. *Nature communications*, *11*(1), 915. https://doi.org/10.1038/s41467-020-14531-6

[10] Zhao, T., Chen, G., Pang, C., Seenoi, P., Papukdee, N., & Busababodhin, P. (2025). Application and performance optimization of SLHS-TCN-XGBoost model in power demand forecasting. *Computer Modeling in Engineering & Sciences*, 143(3), 2883-2917. https://doi.org/10.32604/cmes.2025.066442

[11] Mei, F., Zhang, J., Lu, J., Lu, J., Jiang, Y., Gu, J., ... & Gan, L. (2021). Stochastic optimal operation model for a distributed integrated energy system based on multiple-scenario simulations. *Energy*, *219*, 119629. https://doi.org/10.1016/j.energy.2020.119629

[12] Gu, Y., Deng, J., Lu, H., Huang, Y., Qiao, J., & Jin, M. (2025, December). A Stochastic Optimization Method for Distribution Network Operation and Maintenance Driven by Load Uncertainty Scenarios. In 2025 IEEE 9th Conference on Energy Internet and Energy System Integration (EI2) (pp. 2437-2442). IEEE. https://doi.org/10.1109/EI268505.2025.11425219

[13] Patel, V., Giri, V. K., & Kumar, A. (2024). Efficient power management strategies for AC/DC microgrids with multiple voltage buses for sustainable renewable energy integration. *Energy Informatics*, *7*(1), 97. https://doi.org/10.1186/s42162-024-00377-5

[14] Jabari, M., Ghoreishi, M., Bragatto, T., Santori, F., Cresta, M., Geri, A., & Maccioni, M. (2025). Advancing hybrid ac/dc microgrid converters: Modeling, control strategies, and fault behavior analysis. *Energies*, *18*(23), 6302. https://doi.org/10.3390/en18236302

[15] Zhi, Y., Sun, T., & Yang, X. (2023). A physical model with meteorological forecasting for hourly rooftop photovoltaic power prediction. *Journal of Building Engineering*, *75*, 106997. https://doi.org/10.1016/j.jobe.2023.106997

[16] Huang, C. J., & Kuo, P. H. (2019). Multiple-input deep convolutional neural network model for short-term photovoltaic power forecasting. *IEEE access*, *7*, 74822-74834. https://doi.org/10.1109/ACCESS.2019.2921238

[17] Qiao, Y., Song, Y., & Huang, K. (2019). A novel control algorithm design for hybrid electric vehicles considering energy consumption and emission performance. *Energies*, *12*(14), 2698. https://doi.org/10.3390/en12142698

[18] Diao, R., Hu, Z., & Song, Y. (2023). Subgradient of cycle-based aging cost function and its application in optimal operation of battery energy storage system with multiple subsystems. *IEEE Transactions on Energy Conversion*, *39*(1), 625-643. https://doi.org/10.1109/TEC.2023.3324917

[19] Chembian, W. T., Senthilkumar, G., Prasanth, A., & Subash, R. (2025). K-means pelican optimization algorithm based search space reduction for remote sensing image retrieval. *Journal of the Indian Society of Remote Sensing*, *53*(1), 101-115. https://doi.org/10.1007/s12524-024-01994-z

[20] Gupta, M. K., & Chandra, P. (2022). Effects of similarity/distance metrics on k-means algorithm with respect to its applications in IoT and multimedia: a review. *Multimedia Tools and Applications*, *81*(26), 37007-37032. https://doi.org/10.1007/s11042-021-11255-7

[21] Zhang, C., Xiang, C., Zhou, P., Qian, H., & Duan, Z. (2026). Optimal scheduling of PV-storage irrigation pump truck by dynamic historical particle swarm optimization. *Agricultural Water Management*, *334*, 110674. https://doi.org/10.1016/j.agwat.2026.110674

[22] Udenwagu, N. E., Oni, A. A., & Ezenwoke, A. A. (2025, April). Improving load balancing in cloud computing for maximum infrastructure utilisation using multi-objective particle swarm optimization algorithm. In *IOP Conference Series: Earth and Environmental Science* (Vol. 1492, No. 1, p. 012005). IOP Publishing. https://doi.org/10.1088/1755-1315/1492/1/012005

[23] Wang, P., Su, Y., Huang, B., Zhu, D., Liu, W., Nedzved, A., ... & Leung, H. (2024). Low-rank tensor completion pansharpening based on haze correction. *IEEE Transactions on Geoscience and Remote Sensing*, *62*, 1-20. https://doi.org/10.1109/tgrs.2024.3405848

[24] Zhang, F., Jiang, H., Liu, F., Hou, T., & Liu, Y. (2026). A metaheuristic study: A partial multitask offloading strategy for vehicular fog computing based on adaptive particle swarm optimization. *Computer Communications*, 108455. https://doi.org/10.1016/j.comcom.2026.108455

[25] Jianhua, L., & Zhiheng, W. (2021). A hybrid sparrow search algorithm based on constructing similarity. Ieee Access, 9, 117581-117595. https://doi.org/10.1109/access.2021.3106269

[26] Aljaidi, M., Jangir, P., Arpita, Agrawal, S. P., Pandya, S. B., Parmar, A., ... & Khishe, M. (2025). A two phase differential evolution algorithm with perturbation and covariance matrix for PEMFC parameter estimation challenges. *Scientific Reports*, *15*(1), 8676. https://doi.org/10.1038/s41598-025-92818-8

APA Citation

You, H., Hua, L., & Su, T. (2026). Economic Dispatch Optimization of Microgrid Based on an Improved Particle Swarm Optimization Algorithm. *International Scientific Technical and Economic Research, 4(3),* 90-124. **https://doi.org/10.67541/ISTAER2627**